HHS Public Access

Author manuscript

ACS Nano. Author manuscript; available in PMC 2023 March 22.

Published in final edited form as:

ACS Nano. 2022 March 22; 16(3): 4666–4683. doi:10.1021/acsnano.1c11374.

Dual Affinity to RBCs and Target Cells (DART) enhances both organ- and cell type-targeting of intravascular nanocarriers

Laura T. Ferguson[†,*], **Elizabeth D. Hood**[‡,*], **Tea Shuvaeva**[‡], **Vladimir V. Shuvaev**[‡], **Maria C. Basil**[†,¥], **Zhicheng Wang**[‡], **Jia Nong**[‡], **Xiaonan Ma**[†], **Jichuan Wu**[†], **Jacob W. Myerson**[‡], **Oscar A. Marcos-Contreras**[‡], **Jeremy Katzen**[†,¥], **Justine M. Carl**[†,¥], **Edward E. Morrisey**[†,¥,¢,£], **Edward Cantu**[§], **Carlos H. Villa**[‡], **Samir Mitragotri**[₴], **Vladimir R. Muzykantov**[‡,#], **Jacob S. Brenner**[†,‡,#]

[†]Department of Medicine, Pulmonary, Allergy, and Critical Care Division, Perelman School of Medicine, University of Pennsylvania, Philadelphia, 19104, USA

[‡]Department of Systems Pharmacology and Translational Therapeutics, Perelman School of Medicine, University of Pennsylvania, Philadelphia, 19104, USA

[¥]Penn-CHOP Lung Biology Institute, Perelman School of Medicine, University of Pennsylvania, Philadelphia, 19104, USA

[¢]Penn Cardiovascular Institute, Perelman School of Medicine, University of Pennsylvania, Philadelphia, 19104, USA

[£]Department of Cell and Developmental Biology, Perelman School of Medicine, University of Pennsylvania, Philadelphia, 19104, USA

[§]Department of Surgery, Division of Cardiovascular Surgery, Perelman School of Medicine, University of Pennsylvania, Philadelphia, 19104, USA

[₴]Wyss Institute for Biologically Inspired Engineering, Harvard University, Cambridge, 02138, USA

Abstract

A long-standing goal of nanomedicine is to improve a drug's benefit by loading it into a nanocarrier that homes solely to a specific target cell and organ. Unfortunately, nanocarriers usually end up with only a small percentage of the injected dose (% ID) in the target organ, due largely to clearance by the liver and spleen. Further, cell-type-specific targeting is rarely achieved without reducing target organ accumulation. To solve these problems, we introduce DART (dual affinity to RBCs and target cells), in which nanocarriers are conjugated to two affinity ligands, one binding red blood cells, and one binding a target cell (here, pulmonary endothelial cells). DART nanocarriers first bind red blood cells, then transfer to the target organ's endothelial cells as the bound red blood cells squeeze through capillaries. We show that within minutes after

[#]Corresponding authors.
[*]Contributed equally

The following supporting information is available online: Schematic of enforced proximity theory, additional DART liposome size and coating characteristics, quantification of additional RBC loading conditions with zoomed-in images of loaded RBC, specificity of DART dual- targeted hitchhiking versus IgG dual- targeted hitchhiking, biodistribution of DART liposomes based on extent of liposome antibody coating, DART organ transfer ratios with anti-PECAM and anti-ICAM endothelial targeting, 20-hour DART biodistribution, and fluorescent microscopy of DART liposomes deposited in murine lung tissue.

intravascular injection in mice, nearly 70 % ID of DART nanocarriers accumulate in the target organ (lungs), more than doubling the % ID ceiling achieved by a multitude of prior technologies, finally achieving a majority % ID in a target organ. Humanized DART nanocarriers in *ex vivo* perfused human lungs recapitulate this phenomenon. Furthermore, DART enhances the selectivity of delivery to target endothelial cells over local phagocytes within the target organ by 6-fold. DART's marked improvement in both organ- and cell-type targeting may thus be helpful in localizing drugs for a multitude of medical applications.

Graphical Abstract

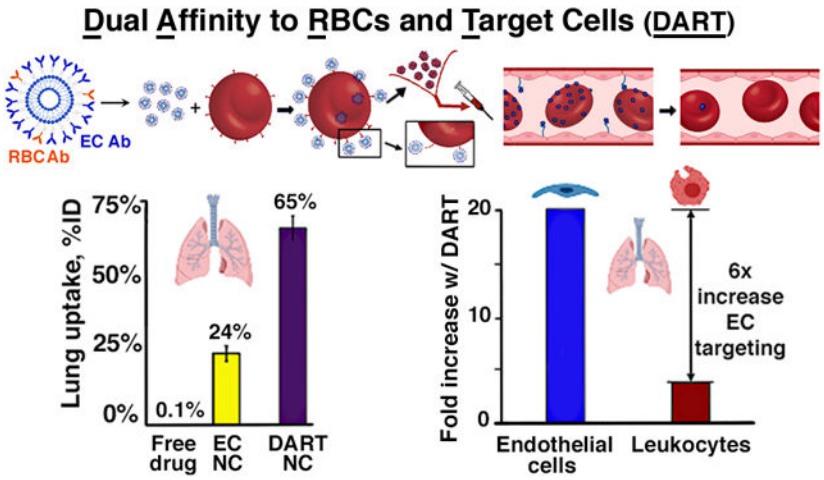

Keywords

nanocarriers; RBC hitchhiking; liposomes; dual targeting; click chemistry; vascular targeting; human lung delivery

Nanomedicine has long held the promise of improving drug efficacy and safety by localizing drugs to both target organs and cells. However, this goal has been very difficult to achieve because the majority of injected nanocarriers are cleared by reticuloendothelial system (RES).[1,2] For example, a meta-analysis of preclinical studies in the largest field of nanomedicine, cancer therapeutics, showed that the median percent of the injected dose (% ID) that was delivered to the target tissue (tumor) was only 0.7 % ID, with the majority going to the RES clearance organs of the liver and spleen.[3] Cancer nanomedicine is not alone in this difficulty. Nearly all intravascularly injected nanocarriers are unable to achieve a majority dose in the target organ, often with closer to just 0.1 % ID reaching the target.[4-9] Therefore, new targeting strategies that increase target uptake and decrease RES clearance are essential.

The oldest and still most common targeting method is ligand-conjugation, in which nanocarriers are covalently bound to affinity ligands (e.g., antibodies) that bind epitopes expressed on cells of interest.[10-12] While ligand-conjugation is still unable to achieve double-digit % ID in the target organ in most cases, one non-RES organ- the lung- has proved to be easier to target. The capillaries of the lungs' air sacs have flow dynamics

advantages that make them easier to target, such as the largest single-organ surface area, low shear stress, and a cumulative blood flow rate equivalent to the rest of the body combined. With such advantages, ligand-conjugated nanocarriers targeted to the endothelial cells of the lungs achieve ~25 % ID.[13-15] Interestingly, 25 % ID seems to be a ceiling for lung targeting efficiency, given this has been achieved with a variety of nanomaterials targeted to a diverse array of endothelial epitopes, including angiotensin-converting enzyme, cell adhesion molecules, and others.[13, 15-21] Although 25 % ID is higher than that achieved in tissues such as tumors, nonetheless, the majority (75 % ID) of these targeted formulations misses even the exceptionally favorable target of the lungs.

To address the targeting problems of ligand-conjugated nanocarriers, we and others have explored new cell-based delivery approaches.[22-31] RBC-hitchhiking, first developed in 2013 by Mitragotri et al, is one such delivery method using red blood cells (RBCs) to shuttle nanocarriers to their target organ.[22] In RBC-hitchhiking, nanocarriers are passively adsorbed onto RBCs *ex vivo* then after intravascular injection, the nanocarriers transfer to the capillary endothelial cells of the immediately downstream organ.[22, 24, 32] This first-pass effect likely involves a mechanical transfer, as the nanocarriers are pressed against the endothelium while carrier RBCs squeeze through the capillaries, and may be enhanced by reduced nanocarrier flow rate.[33] RBC-hitchhiking results in very high % IDs even in difficult organs such as the brain, where RBC-hitchhiking achieved >10 % ID, compared to <1% ID with prior ligand-targeting. Additionally, RBC-hitchhiking marginally improved upon the % ID ceiling in lung targeting (~30 % ID).[24]

Both RBC-hitchhiking and ligand-conjugation have unique strengths and weaknesses, but the two technologies' relative advantages seem to be complementary to each other. RBC-hitchhiking has the advantage of high-efficiency delivery, but has little control over cell-type- or intracellular-target-delivery, only works efficiently with nanocarriers not used clinically, and its mechanisms of RBC-adsorption and nanocarrier transfer are uncertain, which severely limits further engineering. Ligand-conjugation has the advantages of very specific delivery, with easily engineered control of cell-type- and intracellular-delivery, but has relatively low efficiency of delivery.

Therefore, we merge ligand-conjugation and RBC-hitchhiking, to achieve a targeting technology that is highly efficient and engineerable for both organ- and cell-type-targeting. We call this technology DART, Dual Affinity to RBCs and Target cells. DART nanocarriers have 2 affinity ligands: one that binds to RBCs and one that binds the target cell. While prior work has demonstrated targeting with 2 affinity moieties against a single cell type [34-38], DART targets 2 separate cell types. The hypothesized mechanism is that DART nanocarriers rapidly and site-specifically bind to RBCs; then when RBCs abut the target endothelium in capillaries, this enforced proximity between the DART nanocarrier and its target epitope promotes the intentionally stronger binding of the nanocarrier to the target cell, thus transferring the nanocarrier from the RBC to the target cell (Fig 1A, Supplemental Fig 1). This transfer may be facilitated even more in the pulmonary capillary bed due to the low shear stress compared to the systemic circulation.[39-43]

Here we demonstrate DART by targeting the endothelial cells of the lung's alveoli. Alveolar endothelial cells are an important drug target in multiple lung diseases, notably including acute respiratory distress syndrome (ARDS), the alveolar inflammation that kills COVID-19 patients. Alveolar endothelial cells are feasible target cells because they have been studied extensively with many affinity ligands and with RBC-hitchhiking, with an apparent ceiling on delivery efficiency from all prior technologies. We demonstrate DART using the most clinically used nanocarrier, liposomes. As an RBC target epitope, we chose glycophorin A (GPA), which we and others have shown is very abundant (~1 million copies per RBC) and can safely transport RBC cargo drugs such as fusion proteins. [44-48] For binding to the target cells (alveolar endothelial cells), we show DART works with two endothelial epitopes, PECAM and ICAM. We engineered DART liposomes to first bind GPA on RBCs then transfer to the PECAM or ICAM on endothelial cells (Fig 1A). To achieve that transfer, we hypothesized the need for a larger number of PECAM /ICAM affinity ligands than GPA affinity ligands (Fig 1B).

In addition to sequential binding and safe transfer, the majority of DART liposomes (nearly 70% ID) transfer to the lungs in < 2 min after IV injection. This more than doubles the ceiling efficacy of both RBC-hitchhiking and ligand-conjugation. Moreover, DART liposomes provided a 6-fold enhancement of cellular selectivity of targeting to endothelium vs other microvascular cells (local leukocytes). Thus, DART appears to move nanomedicine closer to the long-sought goal of highly efficient and specific organ- and cell-type-targeting.

Results/ Discussion

Construction of nanocarriers for Dual Affinity to RBCs and Target Endothelial Cells (DART).

In choosing how to construct DART nanocarriers for a given target organ, there are 4 major choices: the nanocarrier, the type of affinity ligand, and the target epitopes on both RBCs and target cells. Here, we chose liposomes as the nanocarriers (as they have the most FDA approvals)[49] and monoclonal antibodies as the affinity ligands (similarly have the most FDA approval.[4] For the RBC epitope, we chose glycophorin A (anti-GPA), and for the endothelial epitopes we chose Platelet Endothelial Cell Adhesion Molecule-1 and Intercellular Adhesion Molecule (anti-PECAM and anti-ICAM, respectively). Animal studies have established that after intravascular injection in numerous animal species, cargoes conjugated with anti-GPA bind to RBCs[30], while cargoes conjugated with anti-PECAM and anti-ICAM accumulate in the pulmonary vasculature.[14, 16-18, 21, 50-52] A schematic of the resulting DART liposomes is in Figure 1B. Details on the construction of these and control liposomes is in the Methods section, and quality control data (size, PDI, chromatography traces of antibody conjugation) is in Supplemental Figures 2 and 3.

As DART is a hybrid technology merging RBC-hitchhiking and affinity ligands, we directly compared its efficacy to those individual technologies. Additionally, to understand the mechanism of DART, we have to compare it to multiple controls, which each contain only some components of DART. To more easily discuss these controls, we employ a few acronyms, which are pictorially listed in Figure 1C. In brief, liposomes can have any of 3 antibody combinations, and are named by the cells their antibodies target: 1) RBC-

Targeted (RT) liposomes; 2) Endothelial-Targeted (ET) liposomes; and Dual-Targeted (DT) liposomes, which possess *both* RBC- *and* endothelial-targeting antibodies. Further, these liposome types can be injected in either of 2 protocols: A) "Free" liposomes are injected directly into an animal, without first being exposed to RBCs; or B) RBC-hitchhiking (RH), in which the liposomes are first adsorbed *ex vivo* onto RBCs before injecting into an animal; notably, even without RBC-targeting antibodies, nanoparticles can passively adsorb onto RBCs, as with earlier versions of RBC-hitchhiking.[22, 24] Importantly, when DT liposomes are injected via RBC-hitchhiking (RH), we call them DART liposomes; or, using the nomenclature of the above controls, they can be called DT-RH (in other words DT-RH and DART describe the same thing). While the names of all the controls in Figure 1C are numerous, it is important to keep in mind that they are just controls, for the purpose of elucidating the mechanisms of DART and comparing it to predicate technologies.

To compare DART liposomes with the above controls, we IV-injected radiolabeled versions of each into mice and measured lung uptake 30 minutes later. Figure 1D shows that DART liposomes (DT-RH) achieved a deposition of 65 % ID in the lungs, which is 650-fold greater than the lung uptake of a radiolabeled, free (no carrier) small molecule drug (DTPA). By comparison, free liposomes targeted only to the endothelium (designated as endothelial targeting [ET]), only led to 24 % ID in the lungs. We next assayed whether the other predicate technology, RBC-hitchhiking, can combine with ET liposomes to improve targeting. Such ET-RH liposomes achieved 32 % ID in the lungs. Note that ET-RH liposomes were "passively" adsorbed onto RBCs *ex vivo*, meaning there was no RBC-targeting antibody on the liposome surface, but rather the ET liposomes adsorbed onto RBCs via non-specific binding, which was the basis of the original RBC-hitchhiking technology. Thus, a direct merger of the two top targeting technologies, RBC-hitchhiking and affinity-ligand-only targeting, achieves less than half the lung uptake of DART (DT-RH). Thus, this 65% vs 32% difference between DART and ET-RH shows that DART's benefit is not simply a combination of endothelial-targeting antibody plus RBC-hitchhiking, but also derives organ-targeting benefit from the RBC-targeting antibody. The RBC-targeting antibody by itself (RT liposomes) produced very low lung uptake, showing that to achieve its lung uptake of 65 % ID, DART needs all 3 of its components: RBC-targeting antibody, endothelial-targeting antibody, and an RH protocol.

DART liposome loading onto RBCs is safe and >40x more efficient than prior RBC-hitchhiking techniques.

Having shown the organ-targeting efficacy of DART liposomes, we next set out to assay the safety of DART. We hypothesized that if DART liposomes have an avidity for RBC binding that is too high, they could induce agglutination of the RBCs, forming an aggregate of RBCs that could clog capillaries and lead to toxic RBC lysis. Therefore, we varied the number of RBC-targeting (RT) antibodies per liposome and the number of RT liposomes per RBC, adsorbed the liposomes ex vivo on to mouse RBCs, and assayed for agglutination. We employed a clinical gold standard for agglutination, the round-bottom well assay, in which agglutinated RBCs form a lawn that appears as a large, diffuse red circle, while non-agglutinated RBCs can separately settle to the bottom and therefore appear as a small, uniformly red dot. As shown in Fig 2A's left panel, very high numbers of RBC-targeting

antibodies per liposome (100% of total liposome antibodies) and very high liposome-to-RBC ratios (≥ 2000) do indeed cause agglutination. By contrast, there is a large safety window of up to 25% of surface antibodies targeting RBCs and up to 1000 liposomes/RBC in which there is no agglutination. We confirmed this effect is due to specific binding of the RBC-targeting antibody (anti-GPA) to mouse RBCs, as the same liposomes did not induce aggregation of human RBCs (the anti-GPA antibody is not species-cross-reactive). Thus, DT liposomes can indeed safely adsorb onto RBCs.

A major hurdle for prior targeted nanocarriers has been opsonization of nanocarriers by surface proteins, especially those of the complement family of proteins. Therefore, we investigated whether the dominant opsonin involved in nanoparticle clearance, C3 (complement protein 3), was activated more by DART liposomes than control liposomes. We quantified C3 bonding to nanoparticles by incubating the nanoparticles in mouse serum *in vitro* for 15 minutes, and then measuring by ELISA the production of C3a, which is a protein fragment released upon C3 bonding to a surface (Fig 2B). Compared to C3a activation by the known complement activator cobra venom factor (CVF), neither RBC-loaded DART liposomes, free DT liposomes, or free DT liposomes plus free RBCs resulted in significant complement activation.

To further optimize DART, we quantified how the number of RBC-targeting antibodies per liposome affects binding of liposomes to RBCs. We tested this in 3 ways on liposomes exposed to mouse RBCs in suspension *ex vivo*. First, in Figure 2C, we measured a classic "immunoreactivity," which is the fraction of RBC-targeted (RT) liposomes bound to RBCs, when the target epitope (GPA on RBCs, which is present in 10^6 copies / RBC) is in *vast excess* of the number of liposomes. This showed that the RBC-binding is specific (human RBCs only bound at a constant background level), and that the vast majority of RT liposomes are able to bind RBCs until the # of RT antibodies per liposome is quite low. Second, in Figures 2D & E, we measured classic "binding curves," in which we measured binding at increasing liposome-to-RBC ratios >>1. DT liposomes displayed specific, dose-dependent, saturable, and efficient loading onto mouse RBCs, achieving binding up to ~700 liposomes per RBC at maximal dose. Affirming the specificity of DARTs, liposomes *without* any RT antibodies (i.e., ET liposomes) showed only a low background binding. This low, background binding is the basis for the non-specific adsorption used in the original RBC-hitchhiking technology.[22] DT liposomes containing <25% RT antibody bound to RBCs efficiently (Figs 2D & E) without evidence of agglutination (Fig 2A). Last, we tested the effect of extended incubation, finding that when approximately 200 liposomes were added to washed RBC, overnight incubation did not significantly increase DART liposome loading onto RBC (Supplemental Fig 4).

To further quantify DART's RBC-binding, we used fluorescent liposomes to compare the binding of RBCs to DT vs ET liposomes. DT liposomes coated with 10% anti-GPA and 90% anti-ICAM were compared to ET liposomes coated by 100% anti-ICAM. Microscopy shows that DT liposomes provide higher and more homogenous RBC loading than ET liposomes (Fig 2F, insets; Supplemental Fig 5). Flow cytometry showed that DT liposomes bind to 99.7% of RBCs in suspension, i.e., practically to every RBC (Fig 2F) By contrast, almost 30% of RBCs incubated with ET liposomes remained unbound (Fig 2F), which fits with the

highly variable loading seen in earlier RBC-hitchhiking studies.[24] Additionally, the median fluorescence intensity (MFI) of DT liposome-loaded RBCs (DT-RH; i.e., DART) dwarfed the signal of ET loaded RBCs (i.e., traditional RBC-hitchhiking), by nearly 43-fold. Thus, compared to earlier RBC-hitchhiking, DART provides more uniform nanocarrier loading onto RBCs and a >40-fold higher efficiency.

DART liposomes safely dissociate from RBCs *in vivo* and efficiently localize to the target organ.

Having evaluated the safety and optimal design of DART during the *ex vivo* RBC-loading stage, we next evaluated these features during *in vivo* transfer of the liposomes to the target organ. Our hypothesis was two-fold: First, we hypothesized that optimized DART liposomes effectively bind to pulmonary endothelial cells and allow the carrier RBCs to safely leave the capillaries and circulate like normal RBCs. Second, we hypothesized that if the RBC-avidity of DART liposomes is too high, the RBCs could get stuck in the target organ (lungs).

To test these hypotheses, we ^{125}I-labeled each of the 3 types of liposomes described in Figure 1C: RBC-Targeted (RT) liposomes (with anti-GPA antibodies), Endothelial-Targeted (ET) liposomes (here using anti-PECAM), and Dual-Targeted (DT) liposomes containing both ant-GPA and anti-PECAM at a 2.5 to 97.5% ratio. We *ex vivo* loaded these liposomes onto ^{51}Cr-labeled RBCs, then IV-injected the liposome-loaded RBCs into mice, and sacrificed for biodistribution 30 minutes later.

Tracing of ^{125}I reveals that ET-RH liposomes, but not RT-RH liposomes, accumulate in lungs (Fig 3A). This expected outcome likely reflects direct endothelial targeting of ET liposomes, typical of anti-PECAM conjugates.[13, 21, 50] Most importantly, DART uptake in lungs doubled that of ET-RH liposomes (Fig 3A). Shown in Supplemental Figures 6 & 7, this lung accumulation is specific to DT liposomes directed against RBC and endothelial cells, as the lung targeting is ameliorated when nonspecific IgG replaces the endothelial ligand. Thus, somewhat surprisingly, DT-RH liposomes are more effective at delivery to the pulmonary vasculature, even though their number of endothelial-targeting antibodies (anti-PECAM) is actually lower than ET liposomes. This demonstrates the surprising power of adding just a small fraction of RBC-targeting antibodies.

Tracing of ^{51}Cr shows that the carrier RBCs remain in blood circulation without retention in the lungs (Fig 3B). Taken together with ^{125}I DT liposome data, this indicates that DT (DART) liposomes transfer from carrier RBCs to the lungs (Fig 3B *inset*). The transfer is fast: ^{125}I-labeled DT liposomes, but not ^{51}Cr-RBCs, show pulmonary uptake that peaks immediately post-injection then begins to clear from the lungs within 20 minutes (Fig 3C). Indeed, the blood level of ^{51}Cr-RBCs, but not of ^{125}I-DT liposomes, increases over time after injection (Fig 3C *inset*), indicating that the carrier RBCs safely return to the circulation after unloading DT liposomes.

We hypothesized that this transfer of DART liposomes from RBCs to endothelial cells requires the liposomes to have a specific balance of RBC- and endothelial-avidities. This hypothesis suggests that excessive liposome avidity to RBCs may cause the liposome to remain attached to both the endothelial target and the carrier RBCs. Indeed, an increase in

the anti-GPA to anti-PECAM ratio from 2.5 vs 97.5% to 10 vs 90% leads to a large increase of pulmonary uptake of DART liposomes (Fig 3D), but with a concomitant elevation of ^{51}Cr in the lungs (Fig 3D *inset*). In Supplemental Figure 8, this data is represented as liposome ratios (liposomes in lung: liposomes in blood) and lung ratios (liposomes in lung: RBC in lung) over time, further illustrating the observation that too high an amount of RBC-targeting antibody prevents dissociation of the RBCs from the DART liposomes, trapping RBCs in the target organ. At 20 hours, the liposomes have been cleared from the circulation while a fraction remains detectable in the lung and clearance products can be seen excreted in the urine (Supplemental Fig 9). Thus, DART requires optimizing the nanocarriers' ratio of RBC- to endothelial-targeting avidities, but there is clearly a wide parameter range that permits safe and efficient organ targeting of nanocarriers.

Humanizing DART liposomes and testing in *ex vivo* human lungs

To assess the translational potential of DART, we constructed humanized DART liposomes. As with the above mouse studies, the DART liposomes had surface-conjugated endothelial-targeting (ET) antibodies that bind to the endothelial protein PECAM, and RBC-targeting (RT) antibodies that bind to the RBC protein GPA (we also tested an alternative RBC surface protein, Rh). Using binding curves and agglutination assays, we showed that these "humanized" liposomes interacted with human RBCs similarly to the above studies in mice. In particular, Dual Targeted (DT) liposomes exhibited dose-dependent RBC loading, proportional to the fraction of surface RT antibodies on the liposome (Fig 4A). As in the mouse studies, liposomes with very high concentrations of RT antibodies do produce RBC agglutination. However, once again, there is a large window of safety in the parameters of RBC loading that allows for efficient liposome loading onto RBCs, without RBC agglutination.

We next tested DART liposomes in the human pulmonary vasculature, using perfusion of isolated human lungs, as we previously described.[24] Briefly, the lungs were oxygenated and ventilated, and endovascularly cannulated for perfusion of nanocarriers (Fig 4B & C). Human RBCs from a volunteer donor of blood type matched to the test lung were labeled with ^{51}Cr as described, and then loaded with ^{125}I-labeled DT liposomes. DT liposome-loaded RBCs were perfused through the pulmonary artery (Fig 4C). In this setting, emulating first pass vascular uptake, approximately 30 % ID of DT-RH (DART) liposomes were retained in the lungs, markedly exceeding (almost doubling) retention of the carrier RBCs (Fig 4D). This result indicates that the DART approach provides vascular transfer of RBC-loaded dual-targeted liposomes in human lungs.

DART versatility: successful targeting to diverse epitopes

The above studies showed that DART, used to target the endothelial epitope PECAM, works in both mouse and human systems. The next question that arose is whether DART can be generalized to other targeting epitopes. We therefore investigated DART by targeting a second distinct protein expressed on the surface of endothelial cells, ICAM. While PECAM and ICAM share similar names, they are distinct in 2 key ways that could affect DART: PECAM is constitutive while ICAM is inducible with inflammation; and, more importantly, PECAM is found within intercellular junctions, while ICAM is in lipid

rafts on the apical surface.[21, 53, 54] Therefore, we embarked on a diversification of the DART approach by testing dual-targeted (DT) liposomes that utilized anti-ICAM instead of –PECAM antibodies.

We began with *in vitro* assays, showing that DT liposomes containing anti-ICAM behaved similarly to those containing anti-PECAM, with the expected RBC-binding curves (Fig 2D). Next, we loaded anti-ICAM DT liposomes (^{125}I-tagged) onto RBCs (^{51}Cr-labeled), injected them into mice, and measured biodistribution (Fig 5A & B). We compared the results to the typical controls: RBC-targeted (RT) liposomes only possessing anti-GPA antibodies, and endothelial-targeted (ET) liposomes only possessing anti-ICAM antibodies. Once again, DT-RH (DART) liposomes markedly augmented lung delivery, achieving >2x more lung uptake than ET-RH (Fig 5A). Further, DT-RH (DART) did not increase lung retention of the carrier RBCs (Fig 5B). Thus, DART can safely augment delivery to multiple epitopes in the target organ.

To further validate this important generalization of DART, we performed a few additional key controls. First, we compared two different DT liposomes that had different ratios of RBC-targeted (RT) vs endothelial-targeted (ET) antibodies. Interestingly, unlike PECAM targeting, enhancing DT liposome affinity to RBCs via replacing 25% of anti-ICAM by anti-GPA, did not cause RBC retention in lungs (Fig 5B). This shows that the RT-to-ET antibody ratio must be differentially tuned for each target epitope. Next, in mice, we performed “direct” IV injection of the same liposomes as in Figures 5 A & B, but we bypassed loading onto carrier RBCs (hence, “direct” injection of “free” liposomes). As shown in Figure 5C, all liposomal versions containing anti-ICAM (i.e., DT and ET) accumulated in the lungs with similar efficacy (~100 % ID/g), the same value obtained with ET-liposomes that were injected via an RBC-hitchhiking (RH) protocol in Figure 5A. This shows that only the *combination* of DT liposomes *plus* injection via an RBC-hitchhiking protocol can produce the uptake shown in Figure 5A of DT-RH (DART).

Having shown which components of DART are necessary for target uptake in the lungs, we next sought to determine the kinetics of DART (Figure 5D). In the first row Figure 5D, we used DT liposomes in a similar experiment as in Figure 5A, B, & C, but sacrificing the mice for biodistribution analysis at 5, 10, and 20 minutes after liposome injection (instead of 30 minutes, as in Figure 5A, B, C). This row shows that DT-RH liposomes (DART) localize maximally in the lungs by 5 minutes and stay there (5D, top left panel). By contrast, the carrier RBCs used in DART (measured by ^{51}Cr) quickly localize in the lungs, but rapidly leave (Fig 5D, top middle panel). Thus, DART’s delivery of liposomes to the target organ is very fast, but the egress of DART’s carrier RBCs is somewhat slower, with a half-life on the order of 5 minutes. This phenomenon is demonstrated in Supplemental Figure 10 using the ratio of liposomes in the lung compared to blood, which increases over time, and the ratio of liposomes in the lung compared to RBC in the lung, which also increases over time. Taken together, these ratios demonstrate that liposomes move from the blood to the lung and are retained in the lung more than their carrier RBC. The remaining control conditions (“free” liposomes delivery instead of RBC-hitchhiking; ET and RT liposomes) confirm the safety and specificity of DART’s fast liposome delivery to the target organ, and the slightly

slower, safe passage of RBCs out of the target organ. Thus, extensive pharmacokinetics and biodistribution studies are consistent with the originally proposed mechanism of DART.

DART improves cell type-targeting within the organ of interest

The results above show that DART markedly improves targeting to the *organ* of interest. But within that organ, there are multiple cell types, and therefore it is also important to achieve targeting to the *cell type* of interest. Here we have been using DART to target the endothelial cells of the pulmonary capillaries, but within those capillaries also reside numerous marginated leukocytes, which are mostly innate immune cells (e.g., neutrophils and monocytes) that surveil for circulating pathogens.[55-57] We hypothesized that these marginated leukocytes may take up nanocarriers targeted to the lungs, thus preventing the nanocarriers from reaching their intended targets (endothelial cells). We further hypothesized that DART could prevent such uptake by local leukocytes, and improve targeting to the cell type of interest, endothelial cells.

To test these hypotheses, we injected mice with DART liposomes or controls, and quantified which cell types took up the liposomes. We constructed fluorescently labeled dual-targeted (DT) liposomes and compared how they behaved when injected via an RBC-hitchhiking (RH) protocol (i.e., the full DART method) vs via direct injection (no loading onto RBCs). We used DT liposomes surfaced conjugated to 10% anti-GPA and 90% anti-ICAM antibodies. Mice were injected with liposomes and 30 minutes later the lungs were obtained for microscopy and cell flow cytometry. Endothelial cells were defined as CD31+/CD45− and leukocytes were defined as CD31−/CD45+ (flow cytometry cell classification scheme shown in Figure 6A & B).

Confocal microscopy of lungs from mice injected with DART liposomes shows the liposomes localized to the alveolar microvasculature space (Fig 6C, Supplemental Fig 11). Next, we disaggregated the mouse lungs into single-cell suspensions and subjected them to flow cytometry. Among endothelial cells (Fig 6D, *left column*), 85% were liposome-positive in the DART (DT-RH) group (*bottom left pie chart*), vs only 4% after direct injection of “free” DT liposomes (*top left chart*). Thus, DART improves by >20-fold targeting to endothelial cells. By contrast, the leukocyte population (Fig 6D, *right column*) was 45% liposome-positive in the DART (DT-RH) group vs 12% after direct injection of “free” DT liposomes (Fig 6D *right bottom vs right top pie chart*). Comparing the >20-fold vs <4-fold enhancement of targeting to endothelial vs white blood cells reveals that DART enhances 5.6-fold the endothelial-to-leukocyte selectivity in the lungs. Thus, DART not only improves organ-targeting, but also cell type-targeting.

DART displays a low toxicity profile

All new technologies in nanomedicine require in-depth evaluations for potential side effects. Therefore, we investigated for toxicity in the physiological processes most likely to be affected by DART. In particular, we analyzed effects on the 3 organ systems that most intricately interact with DART: blood, pulmonary, and cardiac.

We began by investigating the first potential side effect associated with nanoparticle injection: infusion reaction upon contact of the nanoparticle with blood’s plasma

proteins. In particular, many nanoparticles activate the complement cascade. When the complement protein C3 bonds to nanoparticles' surfaces, it releases soluble products such as the anaphylatoxins C3a and C5a, which contribute to an anaphylaxis-like syndrome called CARPA (complement-activation related pseudoallergy).[58] To assay for such toxic complement activation, we IV-injected mice with DART liposomes or controls, and drew serum 10 minutes later (a time point previously noted to be the peak for C3a and C5a anaphylatoxin concentration after nanoparticle injection).[58, 59] As shown in Figure 7A, an ELISA assay for C3a in serum detected a large increase in C3a concentration in the positive control mice (which received cobra venom factor [CVF]), but DART (DT-RH) and controls (DT liposomes and ET liposomes) did not show any differences in C3a levels compared to naive (no injection) mice. Thus, we showed that DART probably does not induce significant activation of the complement cascade, and certainly no more than the predicate technology of single-targeted liposomes.

We next examined potential effects of DART liposomes on general pulmonary and cardiac function. We focused on these organs because DART liposomes are targeted to the alveoli of the lungs, where oxygenation of the blood occurs. Twenty-four hours after IV-injection of DART liposomes (DT-RH) or controls, we assayed oxygenation saturation in the blood (SpO2%) and breathing rate, both of which are sensitive indicators of pulmonary function. Neither parameter was changed by DART or control liposomes (Fig 7B). Next, we assayed heart rate, because if DART liposomes somehow clogged the pulmonary arterioles, they would increase pulmonary artery pressures and therefore increase heart rate. DART and DT liposomes had no effect on heart rate, though the predicate technology of single-targeted liposomes (ET liposomes) produced a small increase in heart rate. Thus, DART liposomes do not have detectable impact cardiac or pulmonary physiology and function.

To investigate the possible effects of DART on the blood, we performed complete blood counts (CBC) on mice that had been IV-injected with DART liposomes or controls 24 hours prior. Here we found the only detectable side effect of DART, which is a decrease in the hematocrit, which is the percentage of the blood volume occupied by red blood cells (hemoglobin concentration and RBC count are closely related variables) (Fig 7C). The same small decrement in hemoglobin was seen also with the predicate technology of ET liposomes and the other major control of DT liposomes. The reason for this small decrement could either be a decrease in total RBC volume, or an increase in plasma volume. Either way, the fact that this decrement in hematocrit was also seen with single-targeted liposomes (ET) shows this potential side effect is not unique to DART, but perhaps common to any endothelial-targeted nanoparticle. Future investigations are certainly warranted, but beyond the scope of the present study, since it is not a DART-specific side effect.

The CBC also gave information on the other two major populations of blood cells, white blood cells (WBCs) and platelets. As shown in Figure 7D, neither DART nor control liposomes changed the total WBC count, nor any of the individual WBC cell lines (lymphocytes, monocytes, and neutrophils). Such a lack of change in any WBC cell lineage suggests a minimal immune response to DART. Finally, platelets were also unchanged (Fig 7E), which is important because platelet counts are very sensitive to inflammation and major clotting events.

Finally, we examined whether DART perturbed the tissue architecture of their target cells, the endothelium of the lungs' alveoli. In particular, we were looking for damage to the endothelium, or evidence of "RBC aggregates" that could represent RBCs sticking to capillaries, RBC emboli, or RBCs leaking out of capillaries (hemorrhages). To assay these phenotypes, we IV-injected DART liposomes or controls and 24 hours later excised the lungs for histology. As a positive control, we subjected mice to intra-tracheal acid aspiration, which is a common model of acute lung injury, and is known to produce endothelial damage, RBC-containing clots, and hemorrhages.[60] An observer trained in histology, but blinded to the treatment allocations, measured the frequency of RBC aggregates in the lung histology. As shown in Figure 7F, nearly every field of view of the positive control contained RBC aggregates, while such aggregates were much rarer in all the groups receiving liposomes. Notably, there were no statistically significant differences between mice that received DART (DT-RH) vs control liposomes. Thus, DART does not produce any detectable increase in RBC aggregates in the lungs compared to predicate technologies such as single-targeted liposomes (ET), and thus likely does not lead to significant RBC emboli or alveolar hemorrhages. Lastly, we examined the overall tissue architecture, especially for endothelial damage, and did not detect any, as shown by representative images in Figure 7G.

The goal of nanomedicine has long been to localize drug-loaded nanocarriers to a specific organ and/or cell type. The field has made tremendous progress towards this goal, in large part from conjugating ligands onto the surface of nanocarriers. However, in nearly every case, far less than half the nanocarrier ends up in the target organ (unless the target organ is the liver), with values of < 1% being common for targets such as the brain and solid cancers.

To address this and other delivery problems, here we introduced DART, which provides synergy between affinity-ligand-targeting and cell-mediated delivery. We demonstrated four advantages that DART provides over predicate technologies:

First, DART markedly improved *organ-targeting*. Figure 1D compares DART to other carriers and free drug, with the metric being the percent of the injected dose in the target organ (lungs) after 30 minutes in mice. DART (also called DT-RH) delivered to the target organ (lungs) >65% of the injected dose of nanocarriers. Notably, this was 2.5x better than achieved with single-antibody-targeting (Endothelial Targeted, ET liposomes) using the most studied group of lung-targeting antibodies, anti-CAMs. It was also >2x better than passive RBC-hitchhiking (RH; meaning no RBC-binding antibody, just passive adsorption of nanocarriers onto RBCs), even when the RH liposomes included an anti-CAM antibody. Importantly, DART accumulated at >650-fold higher than a hydrophilic small molecule drug. Lastly, DART is the only intravascularly delivered nanotechnology that has been shown to deliver liposomes to the lungs such that the majority (>50%) of the liposomes end up in the target organ.

Second, DART dramatically improved *cell-type-targeting* within the target organ. Figure 6E shows that within the target organ (lungs), DART (DT-RH) nanocarriers had a 5.7-fold higher preference for the target cell type (endothelial cells) than did identical nanocarriers not loaded onto RBCs. This was determined by flow cytometry, comparing the fraction of nanocarrier-positive endothelial cells vs nanocarrier-positive non-endothelial cells, which

were almost exclusively leukocytes (CD45+). It may at first seem surprising that a significant fraction of anti-CAM liposomes are taken up by pulmonary leukocytes, as anti-CAM liposomes have been assumed for decades to exclusively target endothelial cells within the lungs.[19, 20] However, it is well documented that alveolar capillaries have abundant marginated neutrophils and monocytes that reside in the alveolar capillary lumen[56, 57], and these cells express CAMs.[61] Depending on the cargo drug and target disease, it may be highly advantageous for lung-targeted nanocarriers to have much greater specificity for endothelial cells. DART provides such increased cell-type specificity, improving it by 6-fold.

Third, compared to passive RBC-hitchhiking (RH), DART dramatically increased the *efficiency* of adsorbing nanocarriers onto the RBC surface. As shown in Figure 2F & G, compared to passive RH, DART produced 43-fold more nanocarrier signal on RBCs. Importantly, in prior work on passive RH[24], most nanocarrier types had < 10% of the nanocarriers adsorb onto the RBC, which means 90% of the nanocarrier is lost in preparation, thus increasing material costs 10-fold. Further, RH's low efficiency adsorption of nanocarriers onto RBCs is coupled with high variance in the adsorption process, which is not observed with DART. DART's improved efficiency of nanocarrier loading onto RBCs thus makes the technology much less costly and more reproducible.

Fourth, DART can increase the *types of nanocarriers* that work with RBC-hitchhiking. In previous work [24], while passive RH modestly improved lung uptake on the 7 types of nanocarriers tested, only 2 of those produced lung localization comparable to anti-CAM nanocarriers, with the others displaying at least 5-fold lower uptake. The mechanism underlying passive RH's variability between nanocarriers is still unknown. Therefore, it was hoped that by using a more defined binding system for RH, namely the two-antibody system of DART (DT-RH), we could convert a nanocarrier that does not work for passive RH into one that does benefit from RH's several advantages. Indeed, the nanocarriers employed in this paper do not work with passive RH but do work with DART.

Here we chose to employ nanocarriers that were as close to clinical application as possible. For the carrier itself, we chose liposomes, since they are the most clinically employed nanocarrier. These liposomes were conjugated to IgG molecules (the most common ligand employed clinically) via copper-free "click chemistry", chosen because of its advantages for scale-up manufacturing (near 100% efficiency, stoichiometric addition, and no toxins to purify after). When adsorbed passively onto RBCs, these liposomes did not show a significant RH-effect or lung uptake (Fig 5D). However, these liposomes in DART format had 65% of the injected dose go to the lungs. In our prior work[24], we found that liposomes conjugated via SATA-maleimide chemistry do work with passive RH, though delivering to the lungs at half the rate as DART and with an RBC-loading efficiency >10x lower. The fact that passive RH does not work for one out of two common conjugation chemistries illustrates how difficult it will be to further develop passive RH, with its unknown mechanism of RBC-nanocarrier binding. By contrast, DART works via a well-defined mechanism of binding, and can broaden the range of applicable nanocarriers.

In addition to the above 4 numerical advantages, another potential benefit of DART is that it can be *rationally engineered*, rather than relying on unknown mechanisms like passive RH.

DART is composed of multiple components with easily quantifiable properties, namely one ligand that binds the mobile cell and another that binds the target cell. There is tremendous design flexibility, as the ligands can be changed in terms of: target epitopes (e.g., here we showed DART works with both anti-ICAM and –PECAM antibodies), absolute number, ratio of the two ligands, specific affinity (e.g., changing to a different antibody clone), and type of ligand (e.g., changing from mAb to the single chain variable (scFv) format).

One last advantage of DART over predicate technologies lies in the fact that DART delivers to the capillaries without blocking their flow. Numerous studies have IV-injected >5-micron-diameter particles and observed that they mechanically lodge in the lungs' capillary lumens.[62-64] While this mechanical obstruction ("embolization") technique delivers the same magnitude of lung delivery as DART, it comes at a steep price: acutely inducing pulmonary arterial hypertension. Induction of pulmonary arterial hypertension by microparticles is even seen with extremely low-doses / radiotracer doses, causing some microparticle imaging tests to be contraindicated in patients with preexisting lung diseases because of the risk of death.[65] The much higher doses of microparticles needed for treatment regimens are likely to cause lethal pulmonary hypertension. By contrast, one of DART's predicate technologies, passive RBC-hitchhiking, specifically did not induce any pulmonary hypertension when examined in detail in mice.[24] Further, DART does not leave behind in the capillaries the micron-scale RBCs, as shown in Figures 3, 5, 6, 7, & Supplemental Figure 6. Thus, DART provides major safety advantages over the simple-yet-risky technique of microparticle embolization in the lungs.

Beyond demonstrating the advantages of DART over predicate technologies, the present study also provided two key insights into the mechanism of DART, via detailed pharmacokinetic and biodistribution studies. First, delivery to the lungs by anti-CAM nanocarriers or DART is very fast. Lung uptake has reached a maximum by at least 5 minutes post-injection (Fig 5D column 1, row 1). Second, DART's carrier RBCs leave the lung with a half-life of ~5 minutes (Fig 5D column 2, row 1). Thus, DART rapidly delivers the nanocarriers nearly immediately, but the full transfer is not affected for several minutes.

To build upon this initial study of cell-mediated dual ligand targeting, there are two lines of research that will be important to follow-up:

First, investigating the mechanism of DART may provide insights to improve delivery. Our initial hypothesis was that DART simply presses the ligand-targeted nanocarriers against the capillary walls and thereby increases the probability of binding and transfer to the capillaries. However, while this seems likely to improve overall organ delivery, how does DART improve *cell-type* targeting specificity? One potential mechanism could be that adsorption onto RBCs shields nanocarriers from complement opsonization, as the RBC surface has abundant complement regulatory proteins. Without complement opsonization, the DART nanocarriers may not be taken up by pulmonary marginated leukocytes. This and other mechanisms could further aid in improving DART and other delivery systems.

Second, it will be important to test new variations of DART. One particularly interesting variation will be to compare ligand-conjugation using mAbs vs scFvs. Compared to mAbs,

scFvs have binding affinities characterized by relatively high k_{off} rate constants, which may allow faster unloading of DART nanocarriers at their target organ, and this might lessen the amount of optimization that is needed for each DT-RH application.[14, 66] Other important variations will be to test DART targeted to other organs besides the lungs. Likewise, it will be important to test the generalization of DART to other target cell types, including intentionally targeting other carrier cells (e.g., neutrophils) and target cells (e.g., lymphocytes). Additionally, testing DART with other nanocarriers will be important to broaden its use. Finally, after the above optimizations and mechanistic insights, DART nanocarriers can be loaded with drugs, as we have done with very similar antibody-conjugated liposomal formulations in the past [13, 16, 51], and tested in animal models of disease.

Conclusions

In summary, DART provides multiple numerical advantages over prior targeting technologies and, for select applications, moves nanomedicine towards the goal of highly efficient organ- and cell-type targeting.

Methods/ Experimental

Synthesis and characterization of dual targeted liposomes

Particle synthesis—Azide functionalized PEG liposomes were prepared as described previously.[13, 14] Briefly, lipids DPPC (1,2-dipalmitoyl-*sn*-glycero-3-phosphocholine), cholesterol, and azide PEG_{2000} DSPE (1,2-distearoyl-*sn*-glycero-3-phosphoethanolamine-N-[azido(polyethylene glycol)-2000]) (Avanti Polar Lipids, Alabaster, AL) were combined at a phospholipid to cholesterol molar ratio of 3:1 in HPLC grade chloroform. Liposomes requiring ^{111}In radiolabeling include 0.2 mol% DTPA-PE (1,2-distearoyl-*sn*-glycero-3-phosphoethanolamine-N-diethylenetriaminepentaacetic acid), and those requiring fluorescence include 0.5 mol% Top FL-PC (1-palmitoyl-2-(dipyrromethene boron difluoride) undecanoyl-*sn*-glycero-3-phosphocholine) or [TopFl-PE, Rhodamine-PE. Lipid solutions were subjected to a constant stream of nitrogen gas to remove chloroform until visibly dried, then lyophilized for 1-2 h to any remove residual solvent. Dried lipid films were rehydrated with buffer, either sterile PBS or 0.3N metal free citrate at pH 4. This lipid solution underwent 3 cycles of freeze/thaw between liquid N_2 and a 50°C water bath, followed by 10x extrusion cycles through 200 nm polycarbonate filters using an Avanti Mini Extruder (Avanti Polar Lipids). At each stage of particle synthesis and modification we measured particle size, distribution, and polydispersity index (PDI) at 1:125 dilution in PBS using a Zetasizer Nano ZSP. Particle concentration in #/ml was measured using a NanoSight NS300 at a dilution in ultrapure DI water of ~10^4. (Both instruments by Malvern Panalytical, Malvern UK.)

Modification of targeting monoclonal antibodies—As described previously, we synthesized highly stable and homogeneous immunoliposomes for these studies using copper free click chemistry methods.[14] All monoclonal antibodies and control IgG were modified with dibenzylcyclooctyne-PEG4-NHS ester (Jena Bioscience; Thuringia, Germany). The proteins, buffered in PBS and adjusted to pH 8.3 with 1 M NaHCO3

buffer, were reacted for 1 h at room temperature at a ratio of 1:5 antibody/NHS ester PEG_4 DBCO. Post reaction, the mixture was buffer exchanged with an Amicon 10k MWCO centrifugal filter (MilliporeSigma, Burlington MA) to remove unreacted NHS ester PEG4 DBCO by 30 vol washes. The efficiency of DBCO-IgG reaction was determined optically, with absorbance at 280nm indicating IgG concentration and absorbance at 309nm indicating DBCO concentration. Spectral overlap of DBCO and IgG absorbance was noted by correcting absorbance at 280nm. Molar IgG concentration was determined using Beer's Law calculation, with an IgG extinction coefficient of 204,000 L $mol^{-1}cm^{-1}$ at 280 nm. Likewise, the molar DBCO concentration was determined using the DBCO extinction coefficient at 309 nm, 12,000 L $mol^{-1}cm^{-1}$. The number of DBCO per IgG was determined as the ratio. All Ab-DBCO used in these studies had between 2-5 DBCO/Ab.

Monoclonal antibodies modified included those against endothelial targets intracellular adhesion molecule (ICAM-1) and platelet-endothelial cell adhesion molecule (PECAM-1) for both mouse (YN1 (ATCC, Manassas VA) and Mec13 (BioLegend, San Diego CA), respectively) and human (R6.5 (ATCC, Manassas VA) and Ab62 (gift from Dr. Marian Nakada [67]) and those against RBC target GPA both mouse (Ter119, BioLegend, San Diego CA) and human (CD235, Bio-rad Laboratories, Hercules CA), and Rh in human (Bric69, Thermo Fisher/Invitrogen). Whole molecule rat IgG (Thermo Fisher/Invitrogen) was included for controls, and as a non-immune vehicle for ^{125}I to quantify particle localization. Radiolabeling of IgG-DBCO with Na–^{125}I was done using the Iodogen method as already described. For quantification of conjugation individual antibodies in dual preparations, Ab-PEG4-DBCO were further modified with either NHS-Alexafluor 488 or 594 as directed by the manufacturer (ThermoFisher, US), and purified using Amicon filters as described.

Radiolabeling DT liposomes

Liposomes were isotope traced either by inclusion of ^{125}I-IgG/DBCO on the surface of the particle at no more than 10% of total antibody coating or by surface chelation of ^{111}In to DTPA-PE on the particle surface as already described.[14] IgG-DBCO was radio-iodinated with Na–^{125}I using the iodogen method. Surface chelation of ^{111}In was done using metal free conditions to reduce reaction inefficiencies due to metal contamination.^{111}In–Cl3 (Nuclear Diagnostic Products, Cherry Hill, NJ) was diluted in citrate buffer and added to preformed azide 0.2% DTPA liposomes, hydrated with metal-free pH 4 citrate buffer, and reacted for 1 h at 37 °C. The reaction mixture was quenched with 50 mM DTPA to 1 mM final concentration to chelate unincorporated ^{111}In. The radiochemical purity and yield quantified using thin film chromatography (TLC) with mobile phase EDTA 10 μM gamma counting of the aluminum silica strips (Sigma Chemical, St Louis MO). For biodistributions liposomes were labeled at 50-100 μCi/μmol. Liposome samples were buffer exchanged with sterile PBS using Amicon centrifugal filters, followed by targeting ligand conjugation.

All hazardous materials and radioactive samples were handled and disposed according to the guidelines and policies set by the Environmental Health and Radiation Safety department of the University of Pennsylvania.

Ligand conjugation and characterization of dual targeted immunoliposomes

Antibodies were conjugated to liposomes using copper-free click chemistry as previously described.[13, 14] DBCO-functionalized monoclonal antibodies described earlier were incubated with azide-bearing liposomes in 2 mL microcentrifuge tubes from 4 h to overnight at 37°C with rotation. Post incubation mixtures were purified using size exclusion chromatography using Sepharose 4B–Cl (GE Healthcare, Pittsburgh PA) packed in a 20 mL Biorad polyprep column taking 1.0 mL fractions for 25 mL, quantification of binding was done via tracing ligand fluorescence. Dual antibody formulations were characterized individually using different fluorophores conjugated to the proteins directly as described, e.g. Alexafluor 488 for YN1 and Alexafluor 594 for Ter119, with fractions read on a plate reader (Spectramax M2; Molecular Devices, San Jose, CA) or radioactivity (fractions measured on a gamma counter). Efficiency of conjugation reaction is quantitatively defined as the ratio of the area under the curve of the ligand signal in the liposome peak (4.0–6 mL) over the integration of the entire 25 mL elution plotted by signal over elution volume (Supplemental Fig 2 & 3).

Red blood cell (RBC) preparation and liposome loading for *in vivo, in vitro*, and *ex vivo* studies

RBC isolation, purification, and ^{51}Cr labeling—Murine RBC were obtained from male C57BL/6 mice (The Jackson Laboratory, Bar Harbor, ME) by inferior vena cava puncture after anesthesia with ketamine/xylazine (100/10 mg/kg). Human RBC were obtained by sterile venipuncture from healthy adult donors in accordance with the University of Pennsylvania IRB (protocol no. 834383). For *ex vivo* lung perfusion (EVLP) experiments, donor RBC blood type was matched to the blood type for donor lung tissue. Murine and human RBC were treated and washed identically after blood draw. To prevent coagulation, syringes and collection tubes were pre-treated with ethylenediaminetetraacetic acid (EDTA, Sigma Aldrich, St Louis, MO), in DPBS (Corning, Manassas, VA). RBC were purified from WBC, platelets, and serum by centrifugation and washing 2x with DPBS. RBC were either used immediately or resuspended in 5 mM glucose in DPBS (Sigma Aldrich, St Louis, MO) for storage up to 24h at 4°C.

When RBC tracing or labeling was required, RBC were resuspended at 10% hematocrit (hct) in 5 mM glucose and incubated with chromium-51 radionuclide (^{51}Cr, sodium chromate in normal saline, Perkin Elmer Life & Analytical Sciences) for up to 12h at 4C. RBC were washed 2x with DPBS to remove free ^{51}Cr and either used immediately or stored as previously described.

Liposome-RBC loading—RBC were isolated and purified as described. Loading was found to have the highest efficiency when performed at higher RBC concentration (hematocrit) and given at least 90 minutes for binding (Supplemental Fig 4) so liposomes were highly concentrated to maintain an RBC hematocrit of approximately 50% after mixing. Liposome/ RBC mixtures were incubated at 4°C, rotating, for 90 minutes in Axygen maximum recovery microtubes (Corning, Mexico). After incubation with liposomes, RBC were washed 2x with DPBS to remove unbound liposomes then the washes and remaining pellet were measured for radioactivity using a Wallac 1470 Wizard gamma counter

(Perkin Elmer Life and Analytical Sciences-Wallac Oy, Turku, Finland). Liposome loading efficiency was calculated from radioactivity remaining in the RBC pellet after washing divided by radioactivity in the pellet plus washes.

Liposome-RBC binding, immunoreactivity, agglutination, and flow cytometry—A standard agglutination assay was performed as is done clinically.[56] The assay was performed at 2% hct: 20 uL of pRBC with a varied number of liposomes (Fig 2A) were resuspended in 200uL DPBS in a round-bottom 96 well plate (Thermo Fisher Scientific, Denmark). RBC were allowed to settle for 2 hours then observed and photographed for agglutination. Agglutination is assessed visually as the absence of a clean-bordered well-demarcated pellet. Immunoreactivity and binding assays were conducted similarly to loading, with a varied number of liposomes added per individual RBC (Fig 2 & 4). Flow cytometry of loaded RBC was performed on an Accuri C6 (BD Biosciences) and analysis done using FCS express.

Naming conventions for targeted liposomes—Naming conventions used hereafter are diagrammed in Figure 1C. Endothelial targeted (ET) refers to liposomes that are single-targeted to CAM epitopes only. CAMs included here were either Platelet Endothelial Cell Adhesion Molecule (PECAM) or Intercellular Adhesion Molecule 1 (ICAM). RBC targeted (RT) refers to liposomes that are single-targeted to RBC only. Dual targeted (DT) refers to liposomes that are targeted to both a CAM epitope on EC and a surface epitope on RBC. Liposomes that were injected without first being adsorbed onto RBCs are simply called free liposomes.

Animal studies: biodistribution, flow cytometry, microscopy, and toxicity

Biodistribution and pharmacokinetic studies—Naïve C57BL/6 male mice (The Jackson Laboratory, Bar Harbor, ME) anesthetized with ketamine/xylazine (100/10 mg/kg) were injected intravascularly with 1 μmol (0.75 mg) total radioimmunoliposome dual conjugated with targeting ligand against ICAM or PECAM antibody, Ter119 against GPA on the RBC, and ^{125}I-IgG). Each DART dose consisted of approximately 1E8 RBC loaded with 150-300 DT liposomes RBC. Animals were euthanized at designated times after injections; the organs of interest harvested, rinsed with saline, blotted dry, and weighed. Blood samples (~200 ul) were spun down at 500 rcf in a microcentrifuge tube with RBCs separated from plasma. Radioactivity in organs and separated blood components were measured with a Wallac 1470 Wizard gamma counter (PerkinElmer Life and Analytical Sciences-Wallac Oy, Turku, Finland). The gamma data of the ^{125}I and ^{51}Cr (or ^{111}In) measurements and organ weights were used to calculate the tissue biodistribution injected dose per gram. The total injected dose was measured prior to injections, corrected for tube and syringe residuals, and verified to be ≥75% of the sum of the individual measures.

Flow cytometry analysis of dual targeted liposomes and single- cell preparation of lung homogenate—Following intravenous administration of dual targeted liposomes that were either injected freely (direct injection) or loaded *ex vivo* onto RBC, lung tissue was prepared for flow cytometry to determine which cell types liposomes were delivered to. At 30 minutes, a tracheostomy and cannulation were performed then

animals were sacrificed. The right ventricle was cannulated and perfused with cold PBS at 20 cm H2O to flush RBC from the pulmonary capillary bed. Lungs were re-inflated with 0.8 mL digestive enzyme solution (collagenase type 1 (Life Technologies/Gibco), dispase (Corning), DNase1 (Roche) with PBS) and removed from the chest cavity. Harvested lungs were prepared into single cell suspension first by manual chopping with addition of additional digestive enzyme. Samples were incubated in 37C water intermittently vortexed then mixed with fetal bovine serum (Sigma, PA). Homogenate was strained through a 100-micron filter, centrifuged, and resuspended in ACK lysing buffer (Gibco) to remove RBC, then strained through a 40-micron filter on ice, centrifuged, and resuspended in FACS buffer (1% FBS, 1 mM EDTA in PBS, reagents already specified). Cells were fixed then centrifuged and resuspended in FACS buffer for flow cytometry. This single cell suspension was stained for CD45 (Anti-mouse CD45-brilliant violet 421, BioLegend) and PECAM (Anti-Mouse-CD31-APC, Invitrogen, CA). Final resuspension in 2:2000 DAPI was used to exclude dead cells. Flow cytometry was performed on an LSR Fortessa (BD Biosciences) then gated for viability and singlets and analyzed with FlowJo software (FlowJo LLC).

Microscopy studies—For *in vitro* analysis of RBC binding with FITC-labeled TER119-coated liposomes RBC were incubated with the liposomes, washed by centrifugation, adsorbed on glass slides, washed and mounted. In *in vivo* studies animals were sacrificed; lungs were harvested, immersed in OCT, and frozen by liquid N_2. Frozen tissues were cut using Cryostat with 10-20 μm/slice. Samples were fixed with 4% paraformaldehyde for 10 min and permeabilized with 0.3% Triton X-100 for 15 min prior staining with antibodies. Leukocytes were stained with rabbit anti-mouse CD45 antibody (Abcam, #ab10558) followed by Alexa Fluor 647 labeled anti-rabbit IgG. Liposomes were stained with Alexa Fluor 594 goat anti-rat IgG (Invitrogen). Microscopy studies were performed on a confocal laser scanning microscope Leica TCS-SP8 (Leica, Germany) using HC PL APO CS2 63x/1.40 Oil objective and 488/552/638 lasers. Image analysis was performed using Volocity 6.3 Cellular Imaging & Analysis.

Complement activation—ELISA testing was conducted to measure the activated C3a levels *in vitro* and *in vivo* (Fig 2B & 7A). C3a levels were measured by using sandwich ELISA kits from BD Biosciences Company. To measure *in vitro* complement activity, 20 μL fresh serum was incubated with 20 μL immunoliposomes for 15 minutes, then EDTA was added to inhibit further complement activation. To measure *in vivo* complement activity, plasma was collected 10 minutes after iv injection of liposomes or RH- liposomes, then chelated with EDTA and Futhan to inhibit further complement activation. Cobra venom factor (CVF) was used as a positive control, which cleaves all the available soluble C3 to release C3a.

Histology—Whole lungs were fixed by tracheal instillation of neutral buffered 10% formalin at a constant pressure of 25 cmH2O and removed en bloc. Paraffin-embedded 5-μm lung sections were stained with H&E by the Pathology Core Laboratory of Children's Hospital of Philadelphia. Histology was scored by two reviewers for presence of blood clots.

Physiologic measurements and complete blood count (CBC)—Heart rate, oxygen saturation, and respiratory rate were measured 24- hours after iv injection of either DART, PBS, or control DT- liposomes or ET- liposomes using a MouseQx Plus Small Animal Vital Signs Monitor (STARR Life Sciences Corp). Blood was drawn into EDTA and CBC was measured, including: white blood cells, platelets, RBC, hemoglobin (hgb), and hematocrit (hct) using an Abaxis VetScan HM5.

Reproducibility—Animal studies were designed and performed to reduce bias and improve reproducibility. Nє 3 for all experiments, with the exact N listed in each experiment and kept consistent. Mice were randomized across cages by a random number generator. Outcome measures were pre-defined for all experiments. Experiments were blinded when possible: for example, injection could not be blinded because DART is red, while free liposomes appear clear. However, organ preparation for reading of gamma emission was performed by a blinded member of the team. CBC, complement, physiologic data, histology preparation and analysis, and flow cytometry analysis were all performed by blinded team members. Procedures such as sedation, injections, and organ harvesting were performed by the same team members to reduce variability.

Human lung studies

***Ex vivo* lung perfusion—**Human lung tissue was obtained from de-identified lungs that were donated for organ transplant and deemed not suitable for transplantation. All patient specific information was removed before use. This was done under an established protocol with informed consent in accordance with institutional and NIH procedures (PROPEL, approved by University of Pennsylvania Institutional Review Board). This use of deceased donor tissue does not meet the current NIH definition of human subject research; however, all institutional procedures regarding human subject research were followed. The lungs were perfused and harvested by the organ procurement team and kept submerged in PBS at 4°C until use in the lab, within 24 hours of harvest. The lungs were accepted for research if oxygenation, cause of death, and visual assessment was all consistent with normal lung function. We used a modified *ex vivo* lung perfusion (EVLP) protocol.[68] The airway was cannulated and inflated with low pressure oxygen; oxygen flow was continued at approximately 0.8 L/min to maintain gentle inflation. A subsegmental branch of the pulmonary artery was cannulated and perfused with Steen solution for 5 minutes at 20cm H_2O. Green tissue dye was used to test for retrograde flow and identify efflux from the pulmonary vein. RBCs were prepared from healthy donors of matched blood type to procured lung tissue used in each experiment. RBC were labeled with ^{51}Cr and DT liposomes labeled with ^{125}I, a 3mL DT-RH sample was perfused by slow push into the arterial cannulation. This was chased with 3mL of tissue dye to achieve bright staining of the perfused area of tissue. Finally, Steen solution was perfused for 10mg at 20 cm H_2O. All efflux was collected from the pulmonary vein. The lung tissue was then dissected and areas perfused by green tissue dye were measured for retention of liposomes and RBC using ^{51}Cr and ^{125}I signal measured by gamma counter.

Supplementary Material

Refer to Web version on PubMed Central for supplementary material.

Acknowledgements

This study was supported by NIH via grants to VRM (HL157189 and HL143806) and JSB (H138269, HL153510) for EDH, TS, VVS, JWM, OMC, ZW, JN, XM, and JW. EC was supported by HL13522. LF was supported by the National Center for Advancing Translational Sciences of the National Institutes of Health under award number TL1TR001880 and NIH 5T32HL007586-34. The content is solely the responsibility of the authors and does not necessarily represent the official views of the National Institutes of Health.

References

1. Anchordoquy TJ; Barenholz Y; Boraschi D; Chorny M; Decuzzi P; Dobrovolskaia MA; Farhangrazi ZS; Farrell D; Gabizon A; Ghandehari H; Godin B; La-Beck NM; Ljubimova J; Moghimi SM; Pagliaro L; Park JH; Peer D; Ruoslahti E; Serkova NJ; Simberg D, Mechanisms and Barriers in Cancer Nanomedicine: Addressing Challenges, Looking for Solutions. ACS nano 2017, 11 (1), 12–18. [PubMed: 28068099]
2. Moghimi SM; Hunter AC, Capture of stealth nanoparticles by the body's defences. Crit Rev Ther Drug Carrier Syst 2001, 18 (6), 527–50. [PubMed: 11789674]
3. Wilhelm S; Tavares AJ; Dai Q; Ohta S; Audet J; Dvorak HF; Chan WCW, Analysis of nanoparticle delivery to tumours. Nature Reviews Materials 2016, 1 (5), 16014.
4. Allen TM; Cullis PR, Liposomal drug delivery systems: from concept to clinical applications. Adv Drug Deliv Rev 2013, 65 (1), 36–48. [PubMed: 23036225]
5. Elsabahy M; Wooley KL, Design of polymeric nanoparticles for biomedical delivery applications. Chem Soc Rev 2012, 41 (7), 2545–61. [PubMed: 22334259]
6. Gustafson HH; Holt-Casper D; Grainger DW; Ghandehari H, Nanoparticle uptake: The phagocyte problem. Nano Today 2015, 10 (4), 487–510. [PubMed: 26640510]
7. Kiseleva RY; Glassman PM; Greineder CF; Hood ED; Shuvaev VV; Muzykantov VR, Targeting therapeutics to endothelium: are we there yet? Drug Deliv Transl Res 2017.
8. Muro S, Challenges in design and characterization of ligand-targeted drug delivery systems. Journal of controlled release : official journal of the Controlled Release Society 2012, 164 (2), 125–37. [PubMed: 22709588]
9. Paszko E; Senge MO, Immunoliposomes. Current Medicinal Chemistry 2012, 19 (31), 5239–5277. [PubMed: 22934774]
10. Keshavarz A; Alobaida A; McMurtry IF; Nozik-Grayck E; Stenmark KR; Ahsan F, CAR, a Homing Peptide, Prolongs Pulmonary Preferential Vasodilation by Increasing Pulmonary Retention and Reducing Systemic Absorption of Liposomal Fasudil. Mol Pharm 2019, 16 (8), 3414–3429. [PubMed: 31194563]
11. Shamay Y; Elkabets M; Li H; Shah J; Brook S; Wang F; Adler K; Baut E; Scaltriti M; Jena PV; Gardner EE; Poirier JT; Rudin CM; Baselga J; Haimovitz-Friedman A; Heller DA, P-selectin is a nanotherapeutic delivery target in the tumor microenvironment. Sci Transl Med 2016, 8 (345), 345ra87.
12. Torchilin VP; Khaw BA; Smirnov VN; Haber E, Preservation of antimyosin antibody activity after covalent coupling to liposomes. Biochem Biophys Res Commun 1979, 89 (4), 1114–9. [PubMed: 496941]
13. Hood ED; Greineder CF; Dodia C; Han J; Mesaros C; Shuvaev VV; Blair IA; Fisher AB; Muzykantov VR, Antioxidant protection by PECAM-targeted delivery of a novel NADPH-oxidase inhibitor to the endothelium in vitro and in vivo. Journal of controlled release : official journal of the Controlled Release Society 2012, 163 (2), 161–9. [PubMed: 22974832]
14. Hood ED; Greineder CF; Shuvaeva T; Walsh L; Villa CH; Muzykantov VR, Vascular targeting of radiolabeled liposomes with bio-orthogonally conjugated ligands: single chain fragments provide higher specificity than antibodies. Bioconjug Chem 2018.

15. Howard M; Zern BJ; Anselmo AC; Shuvaev VV; Mitragotri S; Muzykantov V, Vascular targeting of nanocarriers: perplexing aspects of the seemingly straightforward paradigm. ACS nano 2014, 8 (5), 4100–32. [PubMed: 24787360]

16. Brenner JS; Bhamidipati K; Glassman PM; Ramakrishnan N; Jiang D; Paris AJ; Myerson JW; Pan DC; Shuvaev VV; Villa CH; Hood ED; Kiseleva R; Greineder CF; Radhakrishnan R; Muzykantov VR, Mechanisms that determine nanocarrier targeting to healthy versus inflamed lung regions. Nanomedicine 2017, 13 (4), 1495–1506. [PubMed: 28065731]

17. Glassman PM; Myerson JW; Ferguson LT; Kiseleva RY; Shuvaev VV; Brenner JS; Muzykantov VR, Targeting drug delivery in the vascular system: Focus on endothelium. Adv Drug Deliv Rev 2020, 157, 96–117. [PubMed: 32579890]

18. Kiseleva R; Greineder CF; Villa CH; Hood ED; Shuvaev VV; Sun J; Chacko AM; Abraham V; DeLisser HM; Muzykantov VR, Mechanism of Collaborative Enhancement of Binding of Paired Antibodies to Distinct Epitopes of Platelet Endothelial Cell Adhesion Molecule-1. PLoS One 2017, 12 (1), e0169537. [PubMed: 28085903]

19. Maruyama K; Holmberg E; Kennel SJ; Klibanov A; Torchilin VP; Huang L, Characterization of in vivo immunoliposome targeting to pulmonary endothelium. J Pharm Sci 1990, 79 (11), 978–84. [PubMed: 2292774]

20. Muzykantov VR; Christofidou-Solomidou M; Balyasnikova I; Harshaw DW; Schultz L; Fisher AB; Albelda SM, Streptavidin facilitates internalization and pulmonary targeting of an anti-endothelial cell antibody (platelet-endothelial cell adhesion molecule 1): a strategy for vascular immunotargeting of drugs. Proc Natl Acad Sci U S A 1999, 96 (5), 2379–84. [PubMed: 10051650]

21. Shuvaev VV; Muro S; Arguiri E; Khoshnejad M; Tliba S; Christofidou-Solomidou M; Muzykantov VR, Size and targeting to PECAM vs ICAM control endothelial delivery, internalization and protective effect of multimolecular SOD conjugates. Journal of controlled release : official journal of the Controlled Release Society 2016, 234, 115–23. [PubMed: 27210108]

22. Anselmo AC; Gupta V; Zern BJ; Pan D; Zakrewsky M; Muzykantov V; Mitragotri S, Delivering nanoparticles to lungs while avoiding liver and spleen through adsorption on red blood cells. ACS nano 2013, 7 (12), 11129–37. [PubMed: 24182189]

23. Batrakova EV; Gendelman HE; Kabanov AV, Cell-mediated drug delivery. Expert Opin Drug Deliv 2011, 8 (4), 415–33. [PubMed: 21348773]

24. Brenner JS; Pan DC; Myerson JW; Marcos-Contreras OA; Villa CH; Patel P; Hekierski H; Chatterjee S; Tao JQ; Parhiz H; Bhamidipati K; Uhler TG; Hood ED; Kiseleva RY; Shuvaev VS; Shuvaeva T; Khoshnejad M; Johnston I; Gregory JV; Lahann J; Wang T; Cantu E; Armstead WM; Mitragotri S; Muzykantov V, Red blood cell-hitchhiking boosts delivery of nanocarriers to chosen organs by orders of magnitude. Nat Commun 2018, 9 (1), 2684. [PubMed: 29992966]

25. Cevaal PM; Ali A; Czuba-Wojnilowicz E; Symons J; Lewin SR; Cortez-Jugo C; Caruso F, In Vivo T Cell-Targeting Nanoparticle Drug Delivery Systems: Considerations for Rational Design. ACS nano 2021, 15 (3), 3736–3753. [PubMed: 33600163]

26. Che J; Najer A; Blakney AK; McKay PF; Bellahcene M; Winter CW; Sintou A; Tang J; Keane TJ; Schneider MD; Shattock RJ; Sattler S; Stevens MM, Neutrophils Enable Local and Non-Invasive Liposome Delivery to Inflamed Skeletal Muscle and Ischemic Heart. Adv Mater 2020, 32 (48), e2003598. [PubMed: 33103807]

27. Lindorfer MA; Nardin A; Foley PL; Solga MD; Bankovich AJ; Martin EN; Henderson AL; Price CW; Gyimesi E; Wozencraft CP; Goldberg JB; Sutherland WM; Taylor RP, Targeting of Pseudomonas aeruginosa in the bloodstream with bispecific monoclonal antibodies. J Immunol 2001, 167 (4), 2240–9. [PubMed: 11490011]

28. Pan D; Vargas-Morales O; Zern B; Anselmo AC; Gupta V; Zakrewsky M; Mitragotri S; Muzykantov V, The Effect of Polymeric Nanoparticles on Biocompatibility of Carrier Red Blood Cells. PLoS One 2016, 11 (3), e0152074. [PubMed: 27003833]

29. Villa CH; Anselmo AC; Mitragotri S; Muzykantov V, Red blood cells: Supercarriers for drugs, biologicals, and nanoparticles and inspiration for advanced delivery systems. Adv Drug Deliv Rev 2016, 106 (Pt A), 88–103. [PubMed: 26941164]

30. Villa CH; Pan DC; Johnston IH; Greineder CF; Walsh LR; Hood ED; Cines DB; Poncz M; Siegel DL; Muzykantov VR, Biocompatible coupling of therapeutic fusion proteins to human erythrocytes. Blood Adv 2018, 2 (3), 165–176. [PubMed: 29365311]

31. Wayne EC; Long C; Haney MJ; Batrakova EV; Leisner TM; Parise LV; Kabanov AV, Targeted Delivery of siRNA Lipoplexes to Cancer Cells Using Macrophage Transient Horizontal Gene Transfer. Adv Sci (Weinh) 2019, 6 (21), 1900582. [PubMed: 31728272]
32. Glassman PM; Villa CH; Ukidve A; Zhao Z; Smith P; Mitragotri S; Russell AJ; Brenner JS; Muzykantov VR, Vascular Drug Delivery Using Carrier Red Blood Cells: Focus on RBC Surface Loading and Pharmacokinetics. Pharmaceutics 2020, 12 (5).
33. Chen YY; Syed AM; MacMillan P; Rocheleau JV; Chan WCW, Flow Rate Affects Nanoparticle Uptake into Endothelial Cells. Adv Mater 2020, 32 (24), e1906274. [PubMed: 32383233]
34. Guo P; Yang J; Liu D; Huang L; Fell G; Huang J; Moses MA; Auguste DT, Dual complementary liposomes inhibit triple-negative breast tumor progression and metastasis. Sci Adv 2019, 5 (3), eaav5010–eaav5010. [PubMed: 30906868]
35. Krasavin M; Sharonova T; Sharoyko V; Zhukovsky D; Kalinin S; Zalubovskis R; Tennikova T; Supuran CT, Combining carbonic anhydrase and thioredoxin reductase inhibitory motifs within a single molecule dramatically increases its cytotoxicity. J Enzyme Inhib Med Chem 2020, 35 (1), 665–671. [PubMed: 32131646]
36. McAteer MA; Schneider JE; Ali ZA; Warrick N; Bursill CA; von zur Muhlen C; Greaves DR; Neubauer S; Channon KM; Choudhury RP, Magnetic resonance imaging of endothelial adhesion molecules in mouse atherosclerosis using dual-targeted microparticles of iron oxide. Arterioscler Thromb Vasc Biol 2008, 28 (1), 77–83. [PubMed: 17962629]
37. Omolola Eniola A; Hammer DA, In vitro characterization of leukocyte mimetic for targeting therapeutics to the endothelium using two receptors. Biomaterials 2005, 26 (34), 7136–44. [PubMed: 15953632]
38. Papademetriou IT; Garnacho C; Schuchman EH; Muro S, In vivo performance of polymer nanocarriers dually-targeted to epitopes of the same or different receptors. Biomaterials 2013, 34 (13), 3459–3466. [PubMed: 23398883]
39. Davies PF, Hemodynamic shear stress and the endothelium in cardiovascular pathophysiology. Nat Clin Pract Cardiovasc Med 2009, 6 (1), 16–26. [PubMed: 19029993]
40. Davies PF; Civelek M; Fang Y; Guerraty MA; Passerini AG, Endothelial heterogeneity associated with regional athero-susceptibility and adaptation to disturbed blood flow in vivo. Semin Thromb Hemost 2010, 36 (3), 265–75. [PubMed: 20533180]
41. Han J; Shuvaev VV; Davies PF; Eckmann DM; Muro S; Muzykantov VR, Flow shear stress differentially regulates endothelial uptake of nanocarriers targeted to distinct epitopes of PECAM-1. Journal of controlled release : official journal of the Controlled Release Society 2015, 210, 39–47. [PubMed: 25966362]
42. Paek J; Park SE; Lu Q; Park KT; Cho M; Oh JM; Kwon KW; Yi YS; Song JW; Edelstein HI; Ishibashi J; Yang W; Myerson JW; Kiseleva RY; Aprelev P; Hood ED; Stambolian D; Seale P; Muzykantov VR; Huh D, Microphysiological Engineering of Self-Assembled and Perfusable Microvascular Beds for the Production of Vascularized Three-Dimensional Human Microtissues. ACS nano 2019, 13 (7), 7627–7643. [PubMed: 31194909]
43. Satariano WA; Ragheb NE; Branch LG; Swanson GM, Difficulties in physical functioning reported by middle-aged and elderly women with breast cancer: a case-control comparison. J Gerontol 1990, 45 (1), M3–11. [PubMed: 2295776]
44. Fraternale A; Rossi L; Magnani M, Encapsulation, metabolism and release of 2-fluoro-ara-AMP from human erythrocytes. Biochim Biophys Acta 1996, 1291 (2), 149–54. [PubMed: 8898876]
45. Magnani M; Pierige F; Rossi L, Erythrocytes as a novel delivery vehicle for biologics: from enzymes to nucleic acid-based therapeutics. Ther Deliv 2012, 3 (3), 405–14. [PubMed: 22833997]
46. Rossi L; Brandi G; Schiavano GF; Scarfi S; Millo E; Damonte G; Benatti U; De Flora A; Magnani M, Heterodimer-loaded erythrocytes as bioreactors for slow delivery of the antiviral drug azidothymidine and the antimycobacterial drug ethambutol. AIDS Res Hum Retroviruses 1999, 15 (4), 345–53. [PubMed: 10082118]
47. Sharma R; Zhao H; Al-Saleem FH; Ubaid AS; Puligedda RD; Segan AT; Lindorfer MA; Bermudez R; Elias M; Adekar SP; Simpson LL; Taylor RP; Dessain SK, Mechanisms of enhanced neutralization of botulinum neurotoxin by monoclonal antibodies conjugated to antibodies

specific for the erythrocyte complement receptor. Mol Immunol 2014, 57 (2), 247–54. [PubMed: 24184879]

48. Zaitsev S; Danielyan K; Murciano JC; Ganguly K; Krasik T; Taylor RP; Pincus S; Jones S; Cines DB; Muzykantov VR, Human complement receptor type 1-directed loading of tissue plasminogen activator on circulating erythrocytes for prophylactic fibrinolysis. Blood 2006, 108 (6), 1895–902. [PubMed: 16735601]
49. Anselmo AC; Mitragotri S, Nanoparticles in the clinic: An update. Bioeng Transl Med 2019, 4 (3), e10143. [PubMed: 31572799]
50. Hood ED; Chorny M; Greineder CF; I SA; Levy RJ; Muzykantov VR, Endothelial targeting of nanocarriers loaded with antioxidant enzymes for protection against vascular oxidative stress and inflammation. Biomaterials 2014, 35 (11), 3708–15. [PubMed: 24480537]
51. Howard MD; Greineder CF; Hood ED; Muzykantov VR, Endothelial targeting of liposomes encapsulating SOD/catalase mimetic EUK-134 alleviates acute pulmonary inflammation. Journal of controlled release : official journal of the Controlled Release Society 2014, 177, 34–41. [PubMed: 24412573]
52. Khoshnejad M; Shuvaev VV; Pulsipher KW; Dai C; Hood ED; Arguiri E; Christofidou-Solomidou M; Dmochowski IJ; Greineder CF; Muzykantov VR, Vascular Accessibility of Endothelial Targeted Ferritin Nanoparticles. Bioconjug Chem 2016, 27 (3), 628–37. [PubMed: 26718023]
53. Ferrer MC; Shuvaev VV; Zern BJ; Composto RJ; Muzykantov VR; Eckmann DM, Icam-1 targeted nanogels loaded with dexamethasone alleviate pulmonary inflammation. PLoS One 2014, 9 (7), e102329. [PubMed: 25019304]
54. Marcos-Contreras OA; Brenner JS; Kiseleva RY; Zuluaga-Ramirez V; Greineder CF; Villa CH; Hood ED; Myerson JW; Muro S; Persidsky Y; Muzykantov VR, Combining vascular targeting and the local first pass provides 100-fold higher uptake of ICAM-1-targeted vs untargeted nanocarriers in the inflamed brain. Journal of controlled release : official journal of the Controlled Release Society 2019, 301, 54–61. [PubMed: 30871995]
55. Doerschuk CM, Leukocyte trafficking in alveoli and airway passages. Respir Res 2000, 1 (3), 136–40. [PubMed: 11667977]
56. Granton E; Kim JH; Podstawka J; Yipp BG, The Lung Microvasculature Is a Functional Immune Niche. Trends Immunol 2018, 39 (11), 890–899. [PubMed: 30253910]
57. Yipp BG; Kim JH; Lima R; Zbytnuik LD; Petri B; Swanlund N; Ho M; Szeto VG; Tak T; Koenderman L; Pickkers P; Tool ATJ; Kuijpers TW; van den Berg TK; Looney MR; Krummel MF; Kubes P, The Lung is a Host Defense Niche for Immediate Neutrophil-Mediated Vascular Protection. Sci Immunol 2017, 2 (10).
58. Szebeni J, Complement activation-related pseudoallergy: a stress reaction in blood triggered by nanomedicines and biologicals. Mol Immunol 2014, 61 (2), 163–73. [PubMed: 25124145]
59. Zamboni WC; Szebeni J; Kozlov SV; Lucas AT; Piscitelli JA; Dobrovolskaia MA, Animal models for analysis of immunological responses to nanomaterials: Challenges and considerations. Adv Drug Deliv Rev 2018, 136-137, 82–96. [PubMed: 30273617]
60. Matute-Bello G; Frevert CW; Martin TR, Animal models of acute lung injury. Am J Physiol Lung Cell Mol Physiol 2008, 295 (3), L379–99. [PubMed: 18621912]
61. Woodfin A; Beyrau M; Voisin MB; Ma B; Whiteford JR; Hordijk PL; Hogg N; Nourshargh S, ICAM-1-expressing neutrophils exhibit enhanced effector functions in murine models of endotoxemia. Blood 2016, 127 (7), 898–907. [PubMed: 26647392]
62. Huo D; Deng S; Li L; Ji J, Studies on the poly(lactic-co-glycolic) acid microspheres of cisplatin for lung-targeting. Int J Pharm 2005, 289 (1-2), 63–7. [PubMed: 15652199]
63. Kanke M; Simmons GH; Weiss DL; Bivins BA; DeLuca PP, Clearance of 141C3-labeled microspheres from blood and distribution in specific organs following intravenous and intraarterial administration in beagle dogs. J Pharm Sci 1980, 69 (7), 755–62. [PubMed: 7391933]
64. Lu B; Zhang JQ; Yang H, Lung-targeting microspheres of carboplatin. Int J Pharm 2003, 265 (1-2), 1–11. [PubMed: 14522113]
65. Ponto JA, Changes in Patterns of (99m)Tc-Macroaggregated Albumin Use Between 2000 and 2015. J Nucl Med Technol 2017, 45 (2), 111–113. [PubMed: 28408704]

66. Greineder CF; Villa CH; Walsh LR; Kiseleva RY; Hood ED; Khoshnejad M; Warden-Rothman R; Tsourkas A; Muzykantov VR, Site-Specific Modification of Single-Chain Antibody Fragments for Bioconjugation and Vascular Immunotargeting. Bioconjug Chem 2018, 29(1), 56–66. [PubMed: 29200285]

67. Nakada MT; Amin K; Christofidou-Solomidou M; O'Brien CD; Sun J; Gurubhagavatula I; Heavner GA; Taylor AH; Paddock C; Sun Q-H; Zehnder JL; Newman PJ; Albelda SM; DeLisser HM, Antibodies Against the First Ig-Like Domain of Human Platelet Endothelial Cell Adhesion Molecule-1 (PECAM-1) That Inhibit PECAM-1-Dependent Homophilic Adhesion Block In Vivo Neutrophil Recruitment. The Journal of Immunology 2000, 164 (1), 452–462. [PubMed: 10605042]

68. Vallabhajosyula P; Korutla L; Habertheuer A; Reddy S; Schaufler C; Lasky J; Diamond J; Cantu E 3rd, Ex Vivo Lung Perfusion Model to Study Pulmonary Tissue Extracellular Microvesicle Profiles. Ann Thorac Surg 2017, 103 (6), 1758–1766. [PubMed: 28242077]

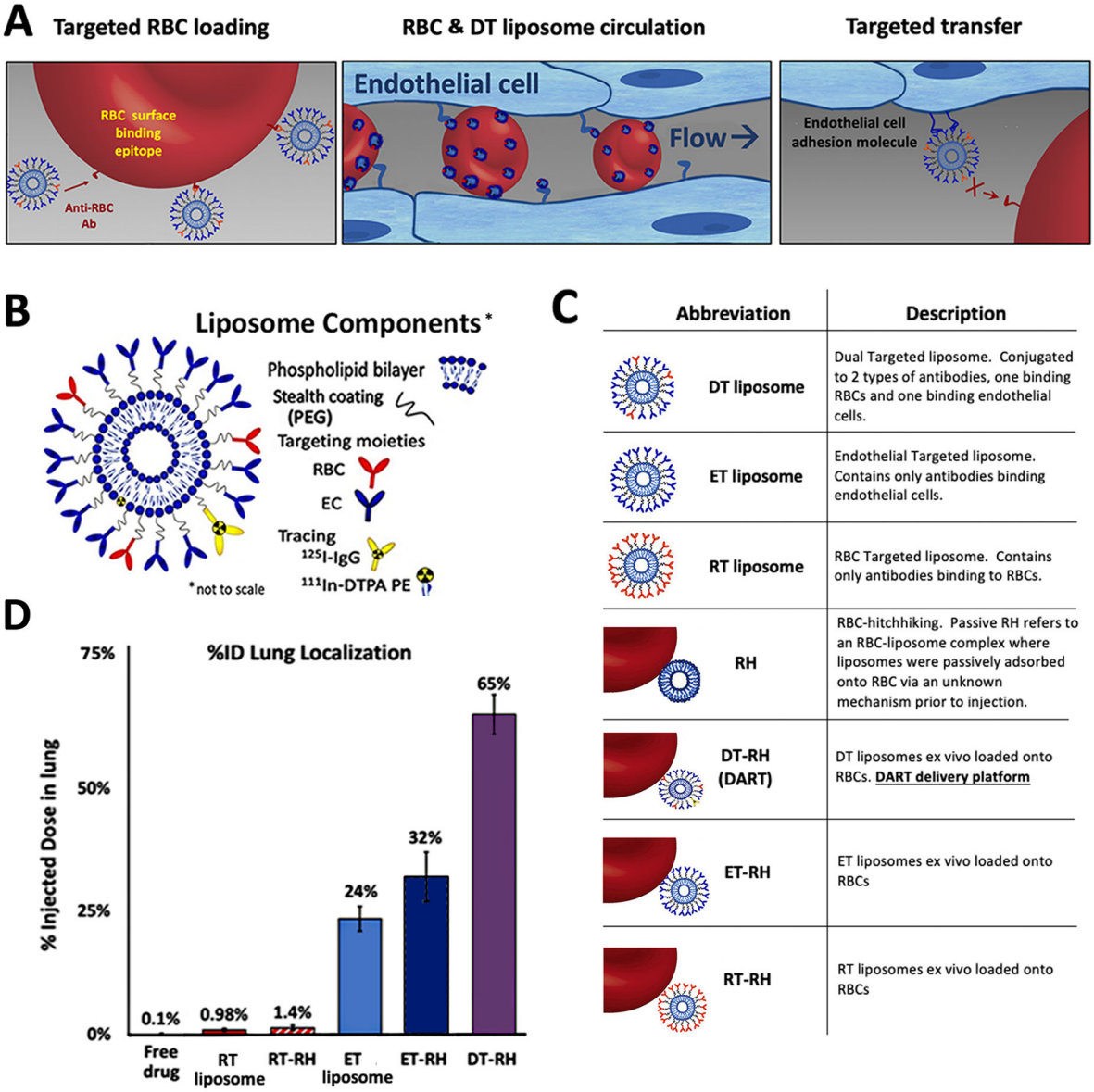

Figure 1. DART more than doubles the efficiency of organ-targeting compared to targeting via affinity-ligands-only and RBC-hitchhiking.

A. The goal mechanism of DART. DART liposomes possess two types of antibodies, one targeting RBCs (red) and one targeting endothelial cells (blue). In the first step (*left panel*), DART liposomes bind to RBCs, via DART liposomes' RBC-targeting antibodies. Next (*center panel*), RBCs transit to the first downstream capillary bed, which for IV injections is the lungs. There the RBCs squeeze through narrow capillaries, increasing the probability of interaction between DART liposomes' endothelial-targeting antibodies and endothelial epitopes. DART liposomes are designed to have many more endothelial-targeting antibodies than RBC-targeting antibodies, so the DART liposomes stay with the endothelium while the RBCs flow past (*right panel*). **B.** DART liposome components, including the two radiolabeling methods (DTPA-^{111}In & IgG-^{125}I); not to scale. **C.** Nomenclature for DART, predicate technologies, and controls. Liposomes can have 3 antibody combinations: RT

= RBC-targeted antibody; ET = endothelial targeted antibody; DT = dual-targeted, which contain both RBC- and endothelial-targeted antibodies. There are 2 protocols of injection: “free” liposomes (e.g. DT liposome or RT or ET liposome) are injected without being exposed to RBCs; RBC-hitchhiking (RH) liposomes are first adsorbed onto RBCs, and the RBC-liposome complexes are then injected intravascularly. **D.** *In vivo* lung localization of the above liposomes and controls, measured by % injected dose (%ID) in the lungs at 30 min post IV-injection in mice. DART (DT-RH) liposomes achieved 650-fold higher levels than free drug (here, free DTPA-^{111}In), and >2x higher than a simple combination of ET + RH (ET-RH). Error bars are standard deviation, n>= 4 for all samples. Statistical differences exist at $p<0.005$ between DT-RH and all groups, and none between RT-L and RT-RH by 1-way Anova.

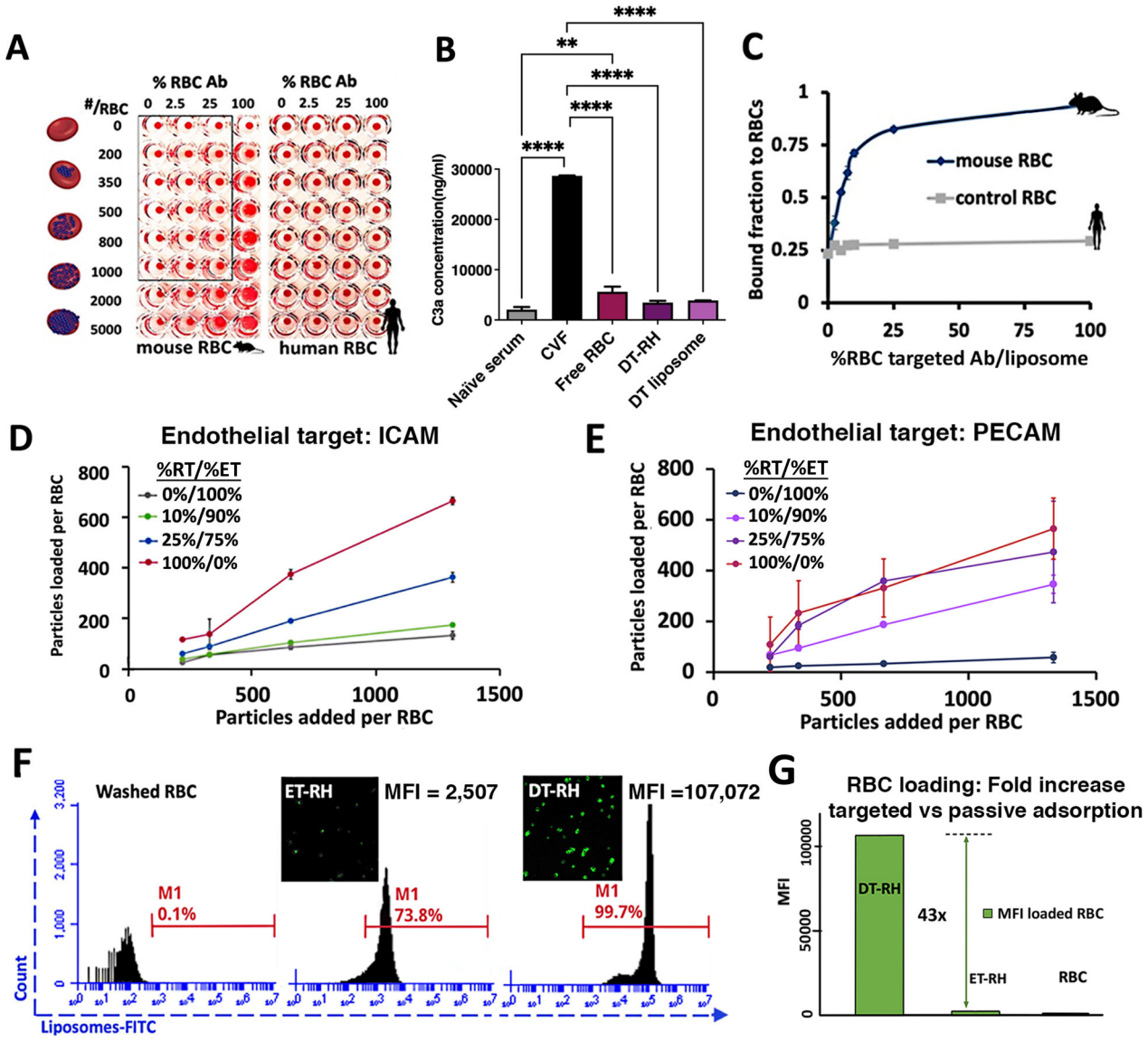

Figure 2. Characterization of liposome to RBC binding by RBC/EC antibody conjugation ratio, coating density, and liposome concentration.

A. Agglutination of RBCs by %RBC Ab coating and # liposomes added. Round-bottom well assay demonstrates the effect of %RBC Ab on liposomes and their concentration in which aggregated RBCs appear diffuse and non-aggregated cells settle into a tight red dot. Image data demonstrate the effect of both the RBC Ab coating density (top left to right, 0-100%) and increased liposome numbers bound (left side top to bottom) affect aggregation of RBCs bound. Human RBCs are tested as a control. RBC samples within the black box define the Ab coating ratios and liposome binding concentration benign to RBC viability with respect to agglutination. **B.** Complement activation *in vitro*, as measured by C3a ELISA. To serum, liposomes +/− RBCs were added, and C3 was measured 10 minutes later. Both DT- RH and free DT liposomes had statistically equivalent complement activation to naïve serum. Cobra venom factor (CVF) is the standard positive control for C3 activation. N=2 biological replicates and 2 technical replicates. Comparisons were done with two-way

ANOVA followed by Tukey's post-test using Prism. P values: **< 0.01, ****< 0.0001. Error bars = SEM. C. ET/DT/RT liposome immunoreactivity shows liposome binding efficiency against a vast excess of RBC binding sites. The binding of 125I labeled liposomes to mouse RBCs was measured against % of mouse RBC Ab on the liposome surface (with the balance of Ab against ICAM). Binding efficiency increases nearly linearly until about 10% RBC mouse Ab, after which binding asymptotically approaches completion. Control binding against human RBCs (gray line) with the same particles demonstrates maximum potential adsorption of non-RBC-targeted liposomes at a given Ab coating. Mouse data N=3, Error = st. dev. D & E. RBC binding to ET/DT/RT ^{125}I labeled liposomes conjugated with EC Ab against ICAM (D) or PECAM (E). Liposome binding to RBC in vitro was measured against the ratio of RBC-to-EC targeting Ab on the liposome surface, with 200 total Ab/ liposome. Graph labels refer to ET= 100% EC targeting, DT= dual targeting at 10%/90% or 25%/75% RT/ET (D), 2.5%/97.5% or 10%/90% RT/ET (E), and RT= 100% RBC targeting. Error bars = st. dev., N= 3 **F &G.** Flow cytometry of RBC loaded with DT-RH liposomes (10%/90%, ICAM targeting) and ET-RH liposomes (100% ICAM targeting) and compared to control RBC. **F.** Flow cytometry was performed on RBC loaded with DT-RH liposomes (99.7% of RBC population binds liposomes) and ET-RH liposomes (73.8% of RBC population binds liposomes) and compared to control RBC. Insets. Fluorescence microscopy of RBC loaded with liposomes. **G.** Mean fluorescent intensity (MFI) quantification of the peaks shown in F indicate 43-fold increase of liposome signal in DT-RH vs ET-RH (ET-ICAM).

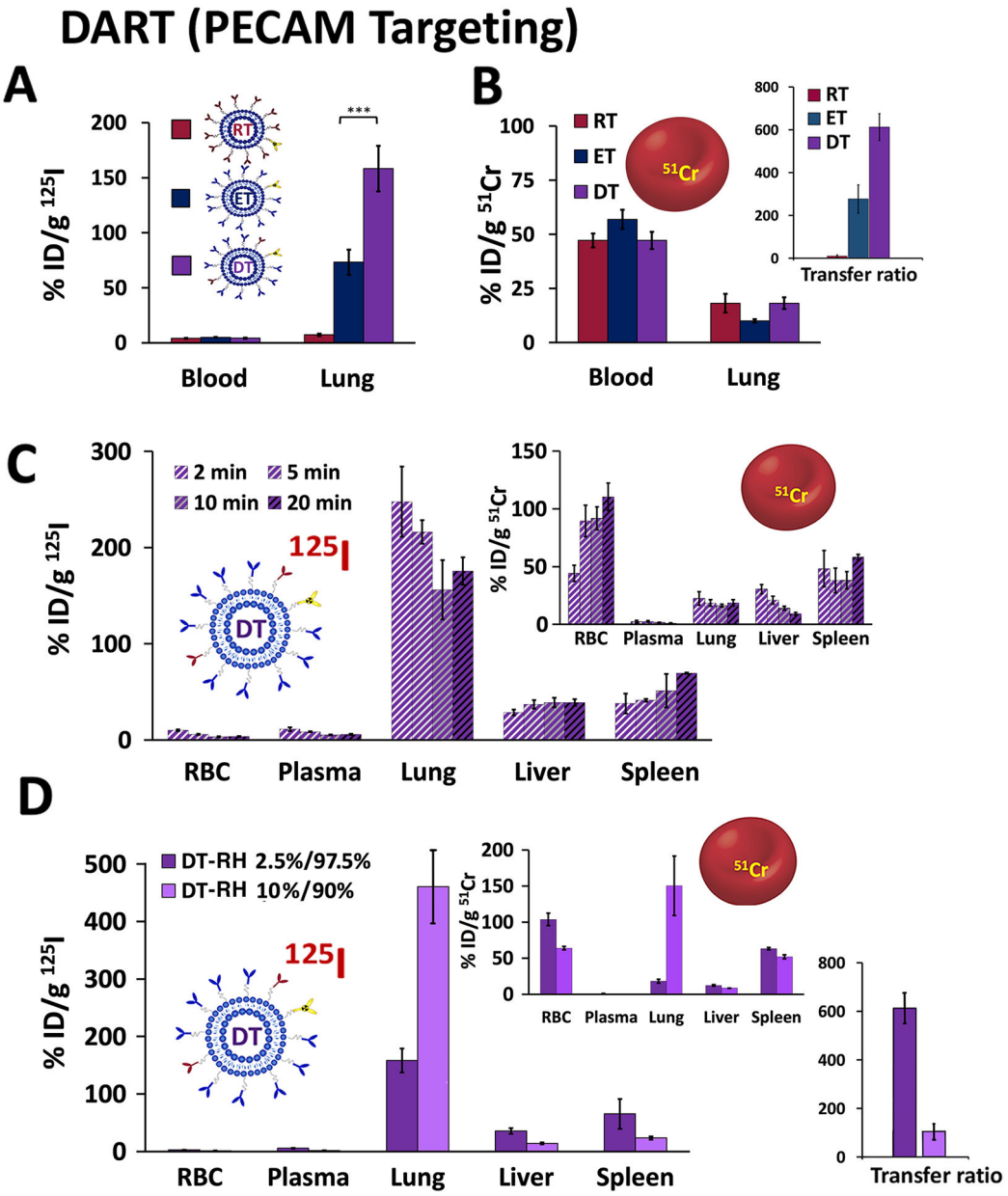

Figure 3. DART liposomes rapidly localize to their lung targets and safely release the carrier RBCs.

A & B. Biodistribution of ^{125}I-liposomes (A) and their ^{51}Cr carrier RBCs (B), using the endothelial-targeting antibody PECAM. Here we approximate concentration of the isotopes in the organ by plotting % ID per gram of tissue (% ID / g), which permits values >100% if an organ is < 1 g. **A.** DT liposomes (DART) achieved > 2x the lung uptake of ET liposomes. DT liposomes add just 5 RBC-targeting antibodies per liposome, keeping 195 PECAM-targeting antibodies (compared to ET liposomes that have 200 PECAM-targeting antibodies), $p<0.001$ by Student T-test. **B.** ^{51}Cr-RBC of RT, ET, and DT liposomes all circulate equally (no statistically significant difference by Student t-test in ^{51}Cr blood concentration) and show no statistically significant difference in lung retention. **Inset** in

B displays the “transfer ratio,” defined as (liposome-to-RBC ratio in lung) ÷ (liposome-to-RBC ratio in blood), measured by their respective isotopes. The transfer ratio describes numerically the transfer of ^{125}I-liposomes from ^{51}Cr RBCs to the target organ (lungs). **C.** Kinetics of DT-RH (DART) biodistribution of ^{125}I liposomes and ^{51}Cr RBC (inset) at 2-20 min after IV injection. DT liposomes’ conjugated antibodies are at a ratio of 2.5% anti-RBC to 97.5% anti-PECAM (total 5 and 195 antibodies, respectively), as was used in A & B. **D.** Evaluation of DART targeting when the ratio of anti-RBC to anti-PECAM antibodies is increased from 2.5%/97.5% to 10%/90% (total 20 and 180 antibodies, respectively). The increase of the RT antibody from 2.5% (dark purple bars) to 10% (light purple bars) results in higher lung localization of liposomes (^{125}I). However, the 10%/90% liposomes (light purple) massively increase the number of carrier RBCs (^{51}Cr) in the lungs. This excessive RBC trapping in the lungs is further quantified by the transfer ratios in the inset. Right: Transfer ratio of 2.5%/97.5% to 10%/90% is 610 to 120. Error bars = st. dev, n=4.

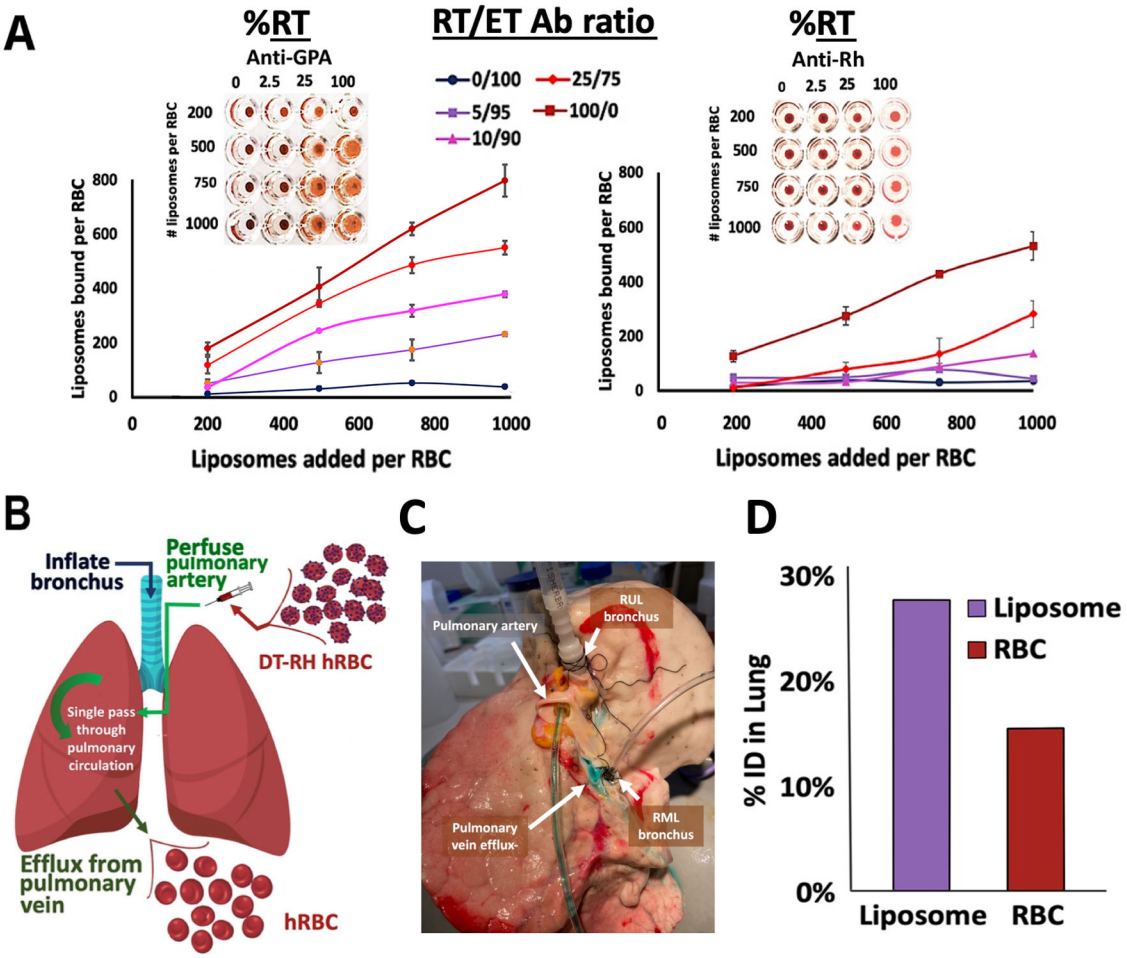

Figure 4. DART liposome proof-of-concept in fresh, perfused, *ex vivo* human lungs.

A. Binding curves and agglutination tests of human RBCs and humanized DART liposomes. Liposomes were functionalized with (1) an endothelial-targeting (ET) antibody binding to human PECAM (the same target protein used in the above mouse studies) and (2) an RBC-targeting (RT) antibody. We compared two RBC surface targets, either binding to human GPA (*left panel*; the same target protein used in the above mouse studies) or Rh (*right panel*). The binding curves are shown for 5 different ratios of RT-to-ET antibodies (legend for the curves is *top center*). The *insets* show RBC agglutination assay results, varying the % RT antibody on the surface of the liposomes, and the # of liposomes per RBC. As with mice, there is a window of safety for these parameters at which no agglutination occurs. Error bars represent st. dev, N=2. **B.** Schematic of *ex vivo* lung perfusion (EVLP). The pulmonary artery is cannulated and perfused using a solution similar to that used in clinical-grade EVLP. The radiolabeled liposomes and RBCs are then injected into the pulmonary artery cannula, allowing a single-pass through the pulmonary capillaries, and then perfusion is continued for 10 minutes, with the perfusate (and radiolabeled material) collected via pulmonary vein efflux. **C.** Fresh human lung prepared for EVLP. Both right upper lobe (RUL) and right middle lobe (RML) bronchi were cannulated for inflation and oxygenation. The pulmonary artery was cannulated for perfusion. Green tissue dye was perfused to confirm adequate cannulation and perfusion through the vasculature with efflux

seen leaving the pulmonary vein. **D**. *Ex vivo* human lungs were perfused using humanized DART liposomes. Liposomes were traced with ^{125}I and RBCs were traced with ^{51}Cr. Of the initial injected dose, 27.5% remained in the lung tissue after perfusion compared to only 15.4% of the carrier RBCs.

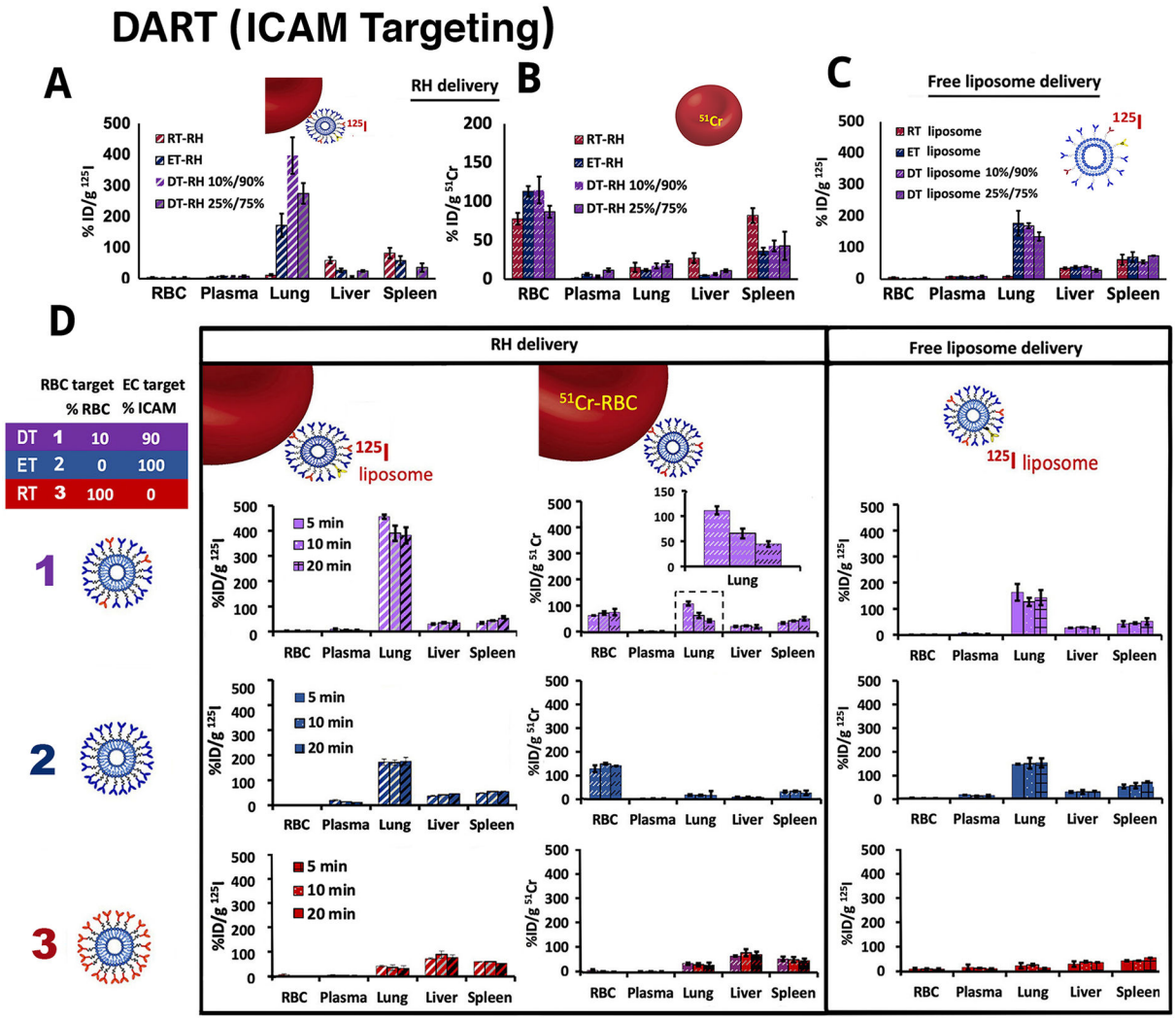

Figure 5. DART works with alternative targeting epitopes to efficiently and rapidly transfer nanocarriers to the target organ.

A & B, Liposomes were constructed similarly to Figure 3A, except the endothelial-targeted (ET) antibody employed was anti-ICAM here, instead of anti-PECAM. Liposomes were either RBC-targeted (RT; red), endothelial-targeted (ET; blue), or dual-targeted (DT; light and medium purple), with the DT liposomes containing either 10% or 25% RT antibody, and 90% or 75% anti-ICAM. These ^{125}I-labeled liposomes were loaded onto ^{51}Cr-labeled RBCs via an RBC-hitchhiking (RH) protocol, IV-injected into mice, and 30 minutes later the mice were sacrificed for biodistribution analysis. (*A*) shows ^{125}I (liposomes), while (*B*) shows ^{51}Cr (carrier RBCs). **(A)** Liposome accumulation in the target organ (lungs) is 2x higher with DT-RH (DART) liposomes (light purple striped) than ET liposomes. **(B)** Carrier RBCs are retained in circulation, not in the lungs. ***C.*** Delivery of “free” liposomes (non-RBC bound) identical to ET/DT/RT-RH shown in *A*. ***D.*** Pharmacokinetics of DART and related controls when the ET antibody targets ICAM and not PECAM. This compares DART condition, (DT, row 1), with controls ET (row 2) and RT (row 3). It also compares delivery by RBC-hitchhiking (RH; columns 1 & 2) versus direct injection of each “free”

liposome (column 3). The inset table on the left side of D describes the % of each antibody used, with the “EC antibody” being anti-ICAM. Y-axis is (%ID/g) and is the same scale for all plots. Most notably, the top left plot shows DT-RH (DART) liposomes are rapidly transferred to the target organ and remain there, while the carrier RBCs (top middle plot) leave the lung overtime. N= 4, error bars are st. dev.

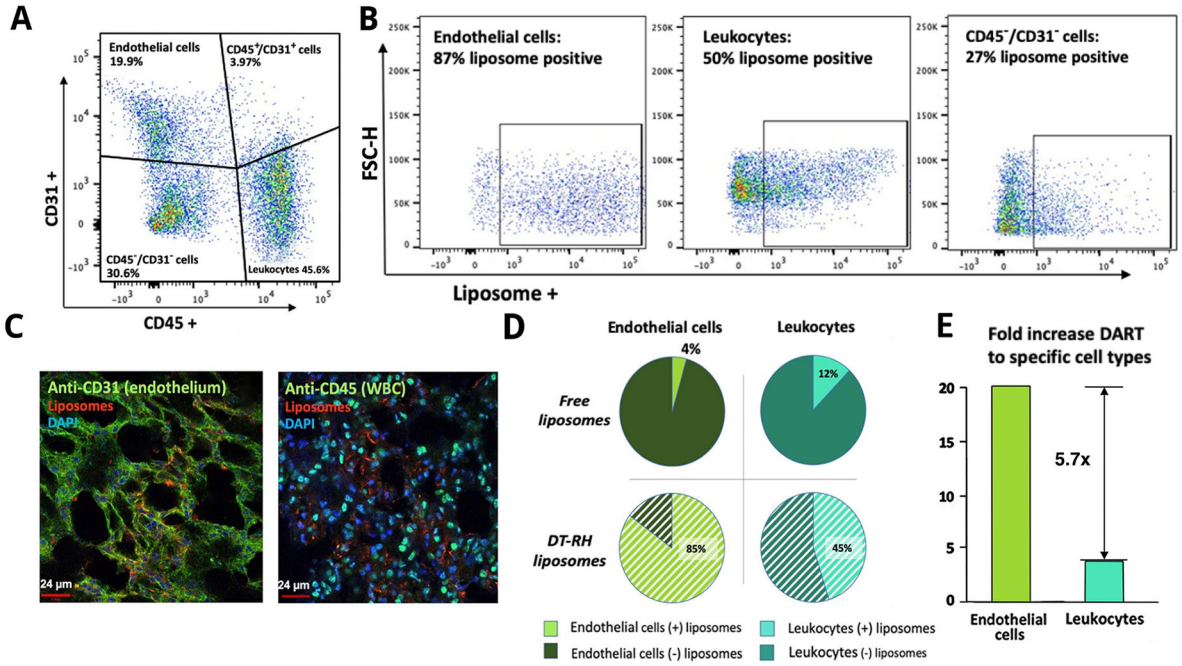

Figure 6. DART improves cell-type-targeting.

Fluorescent dual-targeted (DT) liposomes were constructed that contained 10% anti-GPA and 90% anti-ICAM antibodies. They were injected either directly (“free” liposomes) or via the RBC-hitchhiking (RH) protocol, and mice were sacrificed 30 min later for flow cytometry on single cell suspensions of the lung (A, B, D, E) or lung histology (C). **A.** Dot-plot displaying how cell types were determined by CD31 and CD45 positivity. **B.** Liposome positivity among various cell types. **C.** Fluorescence micrographs indicating association of liposomes (red) with either endothelial cells (left) or leukocytes (right) in the lung after circulation for 30 minutes. **D.** Quantification of flow cytometry data by cell type and liposome positivity. The left column is endothelial cells, and the right is leukocytes. The top row is from mice that had DT-liposomes injected directly (“free” liposomes), and the bottom row is from mice that received DT-RH (DART) liposomes. The lighter colored wedge in each pie chart shows the fraction of liposome+ cells. DT-RH results in a 20-fold increase in endothelial cell targeting and near 4-fold increase in leukocyte targeting. **E.** Analysis of cell localization of DT-RH vs freely injected liposomes. Green bar indicates the increase in endothelial cell localization by fold increase from free liposome injection to DT-RH (DART), and the aqua bar an equivalent calculation of leukocyte localization. Thus, DART produces a 5.7-fold increase in selectivity for endothelial cells vs leukocytes. For flow cytometry, N= 2 biological replicates and 2 technical replicates.

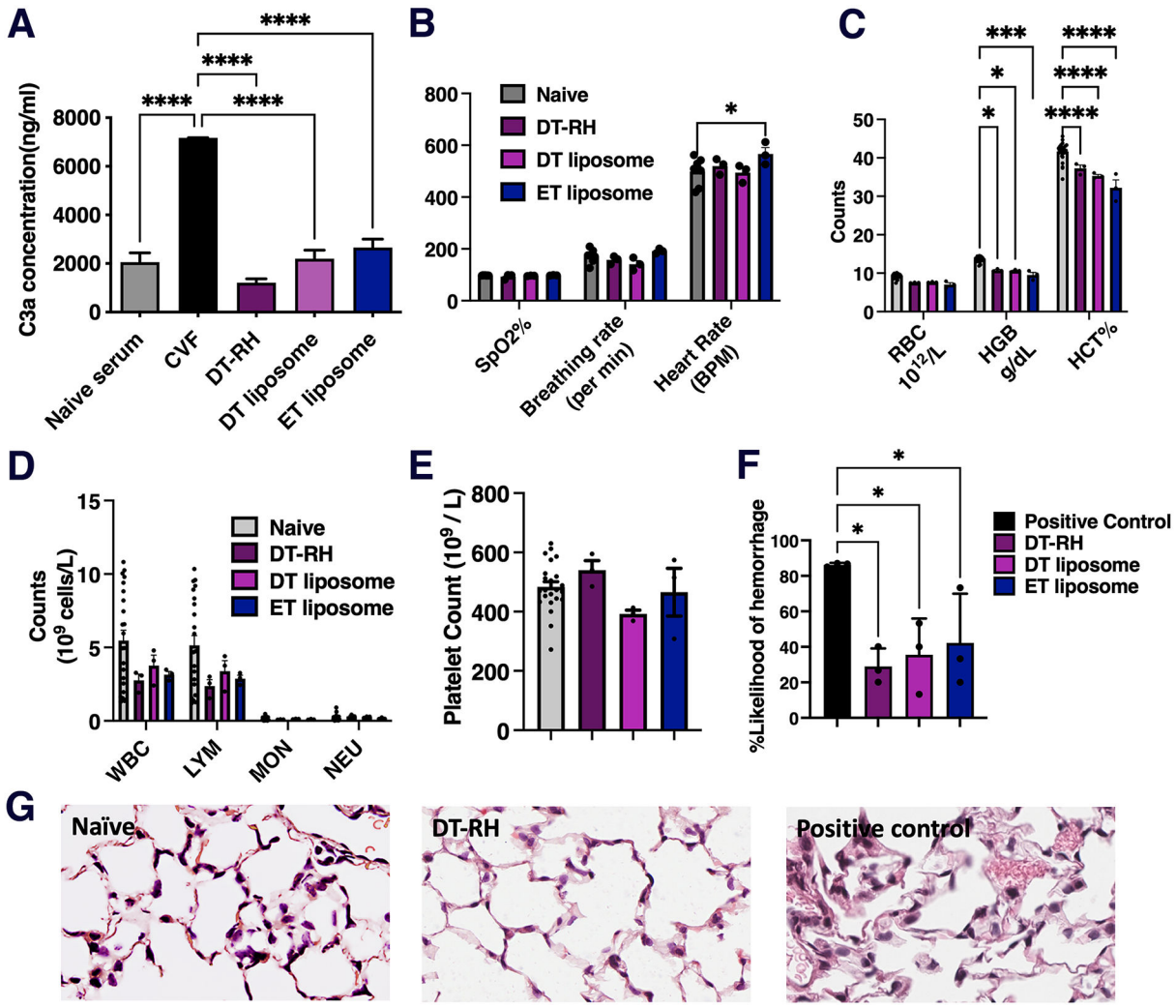

Figure 7. Evaluation of potential side effects of DT-RH *in vivo*.

A. *In vivo* evaluation of complement activation / opsonization after injection of DART liposomes or controls. Liposomes were IV-injected and 10 minutes later serum was drawn and measured for complement activation by C3a ELISA. Cobra venom factor (CVF) is a positive control, inducing C3 cleavage to release C3a. All the liposome formulations lacked significant difference from naive (no injection) controls, including DART liposomes (DT-RH). **B.** Cardiopulmonary physiology of mice 24 hours after IV-injection of DART liposomes and controls. DART liposomes caused no cardiopulmonary changes compared to naive mice, in any of the following: blood oxygenation (measured by oxygen saturation of blood, SpO2), breathing rate, and heart rate. One of the control liposomes (ET liposomes) displayed slightly increased heart rate. **C.** Measurement of RBC count, hemoglobin, and hematocrit at 24 hours after IV-injection of DARTs and controls. All liposome injections, including DART and control liposomes, led to small but statistically significant decreases in these parameters. **D.** White blood cell counts (WBC), measured at the same time as in C, showed none of the liposomes changed total WBC or any of the subsets of lymphocytes, monocytes, and neutrophils. **E.** Platelet counts were also unchanged. **F, G.**

Mice IV-injected with DART liposomes or controls were sacrificed and their lungs removed for histology (H&E staining). As a positive control, separate mice underwent intra-tracheal acid-aspiration, since it is known to induce “RBC aggregates” that represent hemorrhages and clots in the lungs, and those were the two pathologies which most needed investigation for RBC-related nanocarrier delivery. G displays representative images, which show DART-liposome-injected mice had lung histology indistinguishable from naive mice. By contrast, the positive control (acid aspiration) shows multiple RBC aggregates. Blinded observers quantified RBC-aggregate frequency (number of fields in which these were detected), defined as localized collections of RBCs. As shown in F, DART liposomes (DT-RH) and controls all showed significantly less hemorrhages than the positive control, and DART was indistinguishable from the control liposomes. Statistics: A-C: N=3 biological replicates with 2 technical replicates. D, E: N=3 biological replicates. All comparisons were done with two-way ANOVA followed by Tukey’s post-test using Prism; error bars = SEM. * $p < 0.05$; ** $p < 0.01$; *** $p < 0.001$; **** $p < 0.0001$. F: N=3 biological replicates, 3 slides per replicate, 15 distinct fields analyzed per slide.

Video 1.